



CONTRACT NO. A932-099
FINAL REPORT
JULY 1992

Development of Laser Diagnostics Methods for PAH: Phase I

Development of Laser Desorption Laser Photoionization Mass Spectrometry Method for the Screening of Polycyclic Aromatic Hydrocarbons in Soots and Fly Ash

BAL 601-4277
CD 76
WAS
KLS
1992

CALIFORNIA ENVIRONMENTAL PROTECTION AGENCY



AIR RESOURCES BOARD
Research Division

**DEVELOPMENT OF LASER DIAGNOSTICS METHODS
FOR PAH: PHASE I**

**DEVELOPMENT OF LASER DESORPTION LASER
PHOTOIONIZATION MASS SPECTROMETRY METHOD
FOR THE SCREENING
OF POLYCYCLIC AROMATIC HYDROCARBONS
IN SOOTS AND FLY ASH**

**Final Report
Contract No. A932-099**

Prepared for:

Research Division
California Air Resources Board
2020 L Street
Sacramento, CA 95814

Submitted by:

University of California, Davis
Davis, CA 95616

Prepared by:

P.B. Kelly, C.H. Smith and M.K. Young
Department of Chemistry

D.P.Y. Chang
Department of Civil and Environmental Engineering

A.D. Jones
Facility for Advanced Instrumentation

JULY 1992

ABSTRACT

A Laser Desorption Laser Photoionization Mass Spectrometry (LDLPMS) technique has been developed for the direct screening of polycyclic aromatic hydrocarbons (PAHs) in as-received soot and fly-ash samples. The method employs pulsed IR desorption from the surface of particulate matter collected on air-sampling filters, followed by UV laser multiphoton ionization of the desorbed molecules. The ions thus formed are mass-analyzed in a custom-built time-of-flight mass spectrometer. Photoionization of PAH standards at 266 nm produces intense parent molecular ion peaks with little or no fragmentation, allowing identification via molecular weight determination. The application of the method to the detection of PAHs in rice soot samples is demonstrated. The level of detection for PAHs is estimated to be 10-20 ng/sample, which is well within the low resolution target detection limit for ARB Method 429.

DISCLAIMER

"THE STATEMENTS AND CONCLUSIONS IN THIS REPORT ARE THOSE OF THE CONTRACTOR AND NOT NECESSARILY THOSE OF THE CALIFORNIA AIR RESOURCES BOARD. THE MENTION OF COMMERCIAL PRODUCTS, THEIR SOURCE OR THEIR USE IN CONNECTION WITH MATERIAL REPORTED HEREIN IS NOT TO BE CONSTRUED AS EITHER AN ACTUAL OR IMPLIED ENDORSEMENT OF SUCH PRODUCTS."

ACKNOWLEDGEMENTS

Several individuals contributed to this study. Dr. Robert Rosenfeld was instrumental in the conceptualization of the project. Professor Bryan Jenkins provided us with TSP samples of rice straw fly ash for method development. Mr. Ralph Propper of the Research Division has helped us through a number of administrative hurdles since the inception of this project. We are thankful for his assistance and encouragement. Funding for this project was provided in part by the National Institutes of Health Sciences "Superfund" program (Grant 1P42-ES04699).

TABLE OF CONTENTS

1. INTRODUCTION	1
2. EXPERIMENTAL	5
2.1 LDLPMS Instrumentation	5
2.2 Source Region Geometry	10
2.3 Standard PAH Compounds	12
2.4 Mass Calibration of LDLPMS Spectra	12
3. RESULTS	13
3.1 Optimization of the LDLPMS Method	13
3.2 LDLPMS of PAH Standards	22
3.3 LDLPMS of Chlorinated Anthracene Isomers	31
3.4 LDLPMS of Rice Soot Samples	34
4. CONCLUSIONS	41
5. REFERENCES	42
APPENDIX I. LDLPMS Spectra of Standard PAH Compounds	A1
APPENDIX II. GC/MS of Rice Soot Extract	A22

LIST OF FIGURES

FIGURE 1.	Steps involved in the LDLPMS method	2
FIGURE 2.	Schematic diagram of the LDLPMS instrumentation	6
FIGURE 3.	Diagram of the custom-built time-of-flight mass spectrometer	7
FIGURE 4.	Schematic diagram of the event timing in the LDLPMS experiment	9
FIGURE 5.	Diagram of the source region of the time-of-flight mass spectrometer, showing the beam geometries for the IR and UV lasers	11
FIGURE 6a.	Time-of-flight spectra illustrating the effect of IR pretrigger time on ion yield	15
FIGURE 6b.	Effect of IR pretrigger time on integrated intensity of major cluster ion peak from graphite	16
FIGURE 7.	IR-only thermal desorption time-of-flight spectra	17
FIGURE 8a.	Time-of-flight spectra illustrating the effect of UV beam position on ion yield	19
FIGURE 8b.	Effect of UV beam position on the integrated intensity of the major cluster ion peak from graphite	20
FIGURE 9.	Effect of UV beam position on the flight time of the major cluster ion peak from graphite	21
FIGURE 10.	LDLPMS spectra of anthracene obtained at 266 nm	24
FIGURE 11.	LDLPMS spectra of phenanthrene obtained at 266 nm.	26
FIGURE 12.	Detail of LDLPMS spectra of anthracene and phenanthrene obtained at 266 nm, showing low mass carbon fragment patterns	26

LIST OF FIGURES, CONTD

FIGURE 13. Effect of increasing 266 nm UV laser power on the LDLPMS spectra of pyrene	28
FIGURE 14. LDLPMS spectra of anthracene and phenanthrene obtained at 299 nm	29
FIGURE 15. LDLPMS spectra of 1-chloro-anthracene obtained at 266 nm	32
FIGURE 16. LDLPMS spectra of 2-chloro-anthracene obtained at 266 nm	33
FIGURE 17. LDLPMS spectra of rice soot on air-sampling filter obtained at 266 nm	36
FIGURE 18. Detail of LDLPMS spectrum of rice soot showing low mass carbon fragment pattern	37
FIGURE 19. LDLPMS spectrum of rice soot on air-sampling filter obtained at 299 nm	37
FIGURE 20. Effect of IR laser power on the LDLPMS spectra of rice soot obtained at 266 nm	38
FIGURE 21. LDLPMS spectrum of rice soot on air-sampling filter obtained at 266 nm after exhaustive sampling	39

LIST OF TABLES

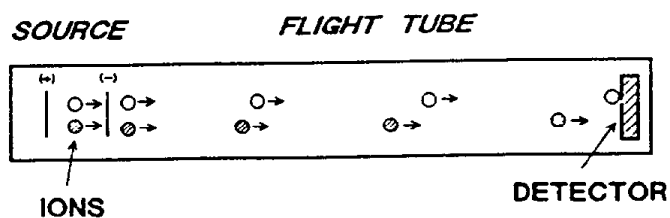
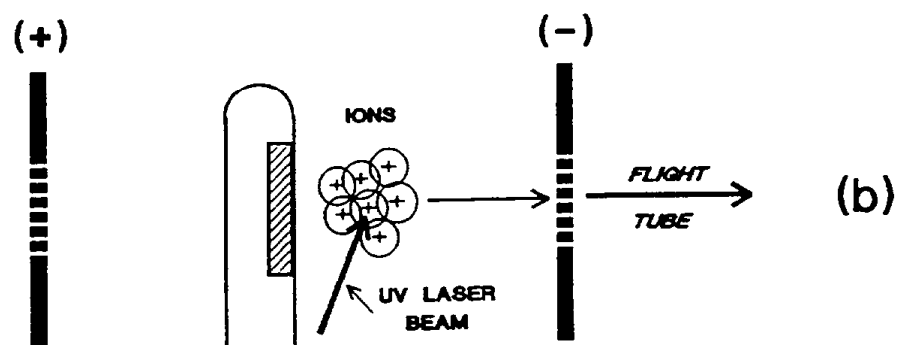
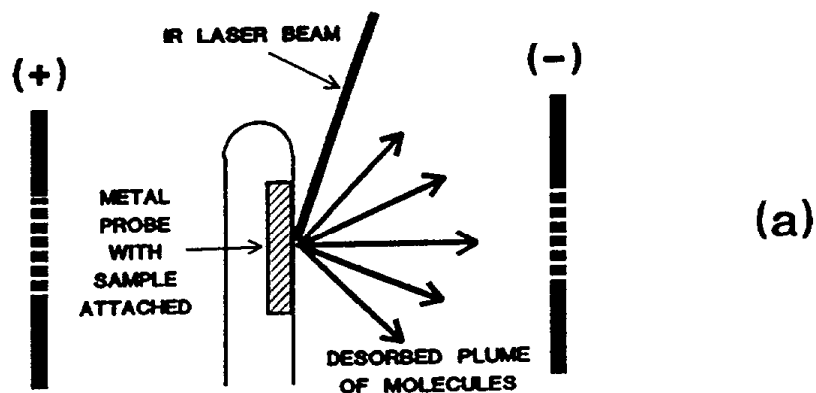
TABLE 1. Properties of Selected PAH Compounds	23
---	----

1. INTRODUCTION

Current methods for the screening and identification of polycyclic aromatic hydrocarbons (PAHs) in soot and fly-ash samples are labor-intensive, time-consuming and expensive. Typically, samples must undergo extraction and separation steps prior to actual analysis by a technique such as mass spectrometry. We have developed a laser desorption laser photoionization mass spectrometry (LDLPMS) technique which provides a means for rapidly screening particulate matter samples for PAHs, with no extraction or separation steps.

The LDLPMS method employs pulsed IR laser desorption followed by pulsed UV laser multiphoton ionization (MPI) of the desorbed neutral molecules. The ions thus formed are mass-analyzed in a time-of-flight (TOF) mass spectrometer, which is ideally suited for a pulsed ionization source. LDLPMS has been demonstrated to be a powerful technique for the analysis of semi- and non-volatile compounds present on a solid substrate (1). We have been able to extend the technique to the analysis of particulate matter collected on air-sampling filter substrates.

The essential steps involved in the LDLPMS method are illustrated in Figure 1. The as-received filter sample is mounted on a metal probe and inserted into the evacuated source region of the TOF mass spectrometer. It is irradiated by a short, focussed pulse of IR light from a CO₂ laser, Figure 1(a), which induces thermal desorption of a small amount of neutral material from the surface of the particulate matter. A short time later, a pulse of UV radiation is directed into the plume of desorbed molecules, Figure 1(b), to form the ions. The wavelength of the UV laser is usually chosen to be in resonance with an electronic transition of the molecules under study. The positive ions thus formed are accelerated into the flight tube of the spectrometer, and detected within a specified time window to generate the mass spectrum, Figure 1(c). The spectra generated by many laser pulses can be averaged together to improve sensitivity and reduce noise.



(c) TOF MASS SPECTROMETER

FIGURE 1. Steps involved in the LDLPMS method. 1(a) The sample is irradiated by a pulsed IR laser beam to desorb material. 1(b) Desorbed neutral molecules are photoionized by a pulsed UV laser. 1(c) Ions are mass-analyzed in a TOF mass spectrometer.

The technique outlined above has several advantages relative to more conventional mass spectral analysis protocols. The sample is analyzed "as-received"; extraction and separation steps, necessary in techniques such as GC/MS, are eliminated. Consequently, very rapid sample turn-around times can be achieved. The TOF mass spectrometer theoretically has no upper mass limit. In practice, the upper limit is determined by elements of the instrument design, but is typically higher than for other types of mass spectrometry.

The key advantage of the LDLPMS method lies in the separation of the desorption and ionization steps. This strategy gives greater control over both processes. In early work in this laboratory, a technique in which a single pulsed UV beam was used to both desorb and simultaneously ionize the sample was developed (2). It was found that the laser powers required to effect desorption from a filter substrate also induced undesirable photofragmentation and photochemical reactions. In the two-step method, the IR laser power can be adjusted to a threshold level to avoid damage to the sample or undesirable side reactions. The power of the UV laser can also be varied. At low powers, "soft" ionization occurs in which predominantly parent molecular ions are formed. This allows compound identification via molecular weight determination. Alternatively, "hard" ionization at higher laser output induces fragmentation of the parent molecules. Identification by characteristic fragmentation patterns may be possible in a similar manner as conventional electron ionization mass spectrometry.

Moreover, the MPI process offers selective analysis in mixtures of compounds. The wavelength of the UV laser can be chosen so that only species which are resonant will be ionized. In the resonance-enhanced MPI process (REMPI), the molecule is promoted into a real intermediate excited electronic state by absorption of the first photon. Absorption of the second photon causes ionization if the sum of the energy of two photons exceeds the ionization potential of the molecule. The probability for ionization is greatly enhanced using two photon REMPI, also known as a [1 + 1] process. The appearance of molecular ions will depend on the overlap between the photon energy and an absorption band of the analyte. Thus a class of compounds such as the PAHs may

be selectively ionized in a mixture by tuning the UV laser wavelength to a particular absorption feature. Isomer-specific analysis is also possible if the isomers have widely separated absorbances. At the present time, there are no libraries of laser photoionization mass spectra available. We are in the process of generating a library for standard polycyclic aromatic hydrocarbons (PAHs) which includes "soft" and "hard" ionization spectra obtained at different UV wavelengths.

In this report, the design, development, and optimization of the LDLPMS method will be discussed. The results of LDLPMS analysis of several PAH standards with 266 nm radiation in both "soft" and "hard" ionization modes will be presented. Two mono-chlorinated anthracene isomers have also been analyzed. Preliminary results for wavelength selectivity are also presented, by comparing mass spectra obtained at 266 nm and 299 nm. Finally, the application of the LDLPMS method to rice soot samples will be demonstrated, and the results compared to the low resolution GC/MS analysis of an extract of the rice soot.

2. EXPERIMENTAL

2.1 LDLPMS Instrumentation

A schematic layout of the experimental apparatus illustrating the important components is shown in Figure 2. At the core of the LDLPMS instrumentation is a custom-built TOF mass spectrometer operating in the linear mode (2). A more detailed diagram of the spectrometer is shown in Figure 3. The sample probe is introduced into the source region through a custom-designed fast load-lock assembly. This feature allows samples to be switched out in minutes without breaking instrument vacuum. The ion optics are housed in the source region. The source region is also fitted with S1 UV quartz and ZnSe optical windows for transmission of the UV and IR laser beams. Positive ions formed between the repeller and extractor plates are accelerated into the field-free flight tube, where they travel at constant velocity to the dual microchannel plate (MCP) detector (Comstock Model CP-602). The detector is mounted in an off-axis geometry, so a deflection potential is applied to the ions as they exit the source region. This off-axis geometry minimizes the transmission of neutral molecules to the detector, thus eliminating a common source of background noise. The source and flight regions are separately pumped by diffusion pumps equipped with cryotrap to achieve an operating vacuum of 10^{-6} torr.

Pulsed IR radiation at 10.6 microns is generated by a Lumonics 934 TEA CO₂ laser with a pulse width of 100 nsec (2 μ sec tail). The beam is attenuated to approximately 20 mJ/pulse and focussed through a 200 mm focal length ZnSe lens into the source region. At the focal point, the beam diameter is 1 mm², yielding power densities of $1-10 \times 10^6$ W/cm² when the laser is operated at a pulse rate of 5 Hz. Power measurements of the IR beam are made prior to focussing using a Scientech Inc. Model 37-4002 power meter.

Pulsed UV radiation is produced by a Q-switched Quanta Ray DCR-3 Nd:YAG laser with a pulse width of 8 nsec. The 1064 nm fundamental is frequency tripled or

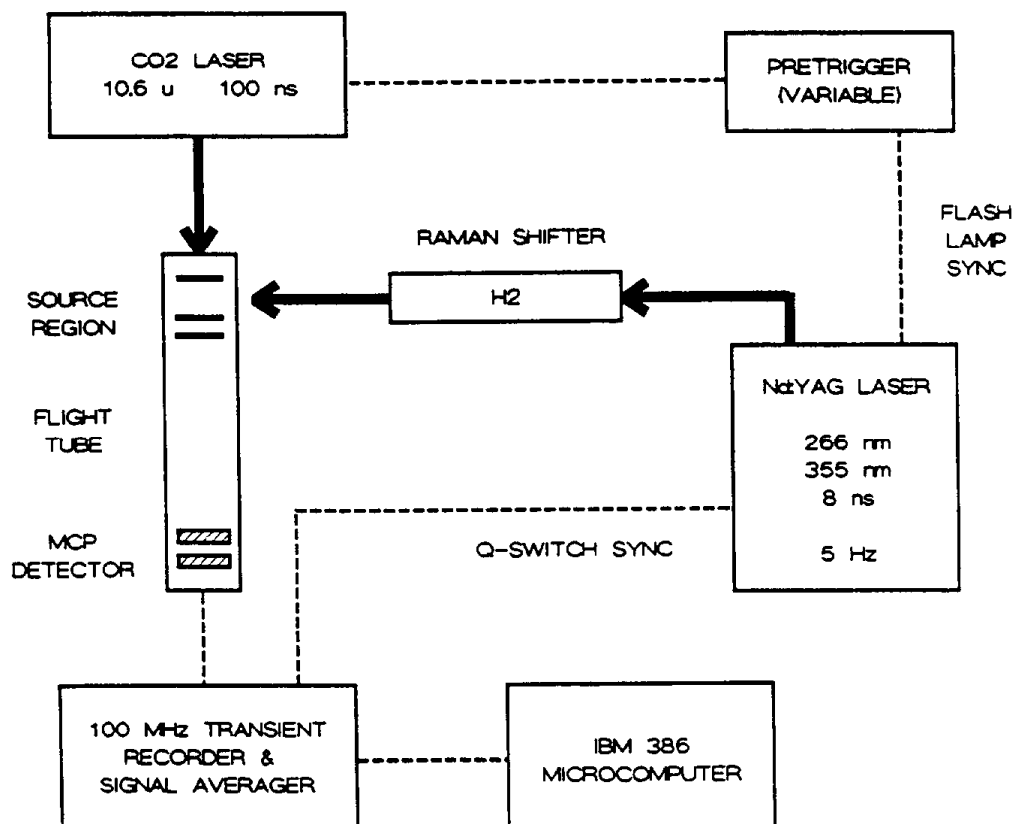


FIGURE 2. Schematic diagram of the LDLPMS instrumentation.

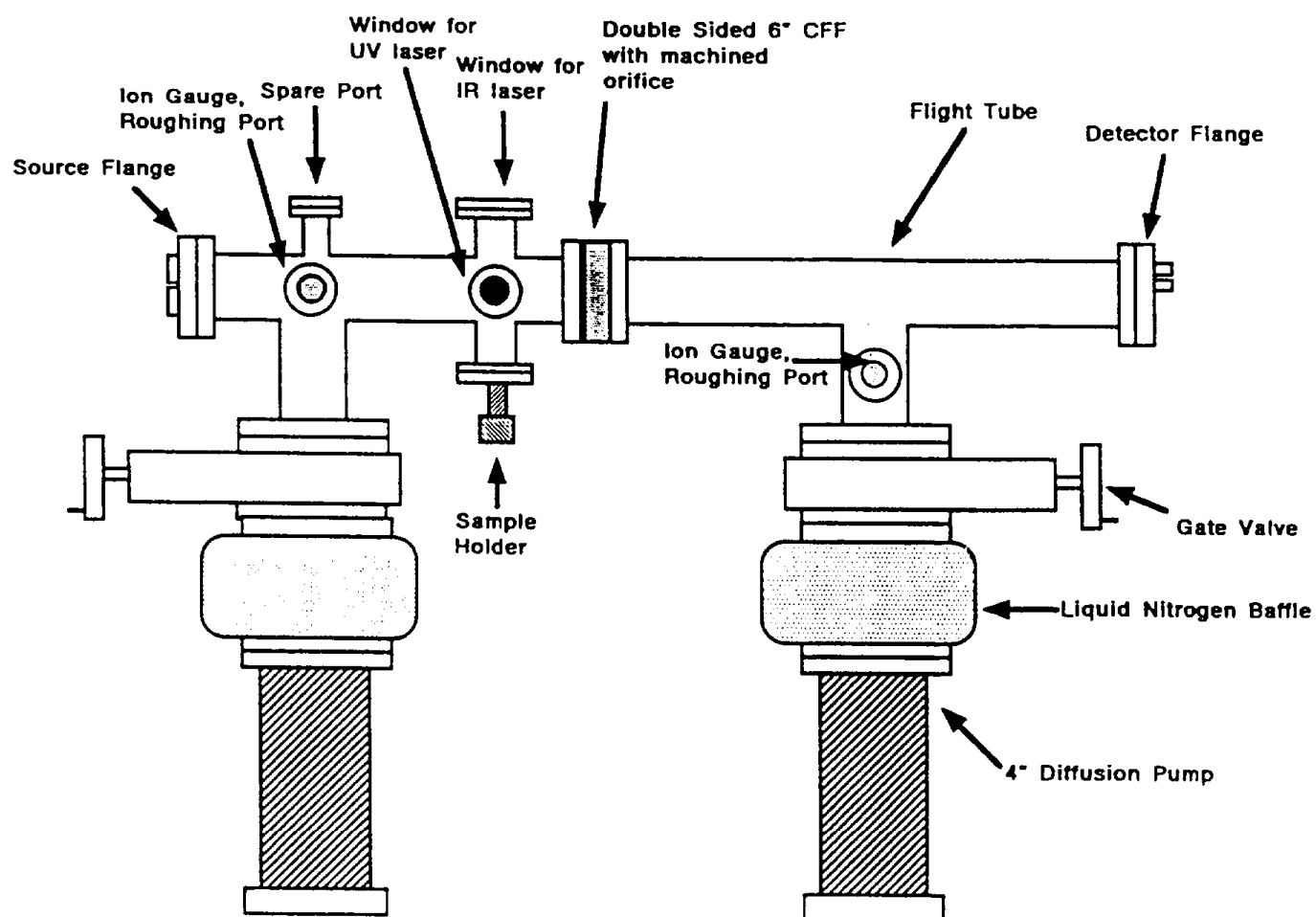


FIGURE 3. Diagram of the custom-built time-of-flight mass spectrometer.

quadrupled to produce radiation at 355 nm and 266 nm respectively. Additional UV wavelengths are obtained using a H₂ gas Raman shifter. Specifically, 266 nm radiation is anti-Stokes shifted to obtain 240 nm radiation, or Stokes shifted to wavelengths of 299 nm and 342 nm. The UV laser beam is narrowed through an iris to a diameter of 2 mm², then focussed through a 190 mm focal length S1 UV quartz lens into the source region. The beam diameter is 0.25 mm² at the focal point. The power density is estimated to be 10⁴ - 10⁵ W/cm² when the laser is operated at a pulse rate of 5 Hz. A UV photometer capable of measuring the relatively low UV powers used in the LDLPMS technique was not available during the period these experiments were performed, but has since been acquired. The beam paths of both lasers in the source region is discussed below.

The current generated at the MCP detector is 50-ohm terminated into a 100 MHz transient recorder (DSP Model 2001AS Transient Recorder) and digitized with 8-bit precision. Typically, 32 KWord scans with a sampling interval of 10 nsec are collected, corresponding to a time window of 40 μ sec. Multiple shots, typically 100 to 500 laser pulses, are signal averaged (DSP Model 4101 Averaging Memory), then transferred by a CAMAC interface to an IBM-clone 386 microcomputer. Data acquisition and subsequent analysis is controlled by software developed in-house. The raw mass spectrum data consists of intensity versus flight time. This is converted and stored as intensity versus flight time squared, since this quantity is proportional to mass.

The signals required for event synchronization in the LDLPMS experiment are generated primarily by the Nd:YAG laser, which is operated at a pulse rate of 5 Hz. A detailed timing diagram is given in Figure 4. Time $t=0$ corresponds to the firing of the flashlamps in the Nd:YAG laser. The flashlamp sync is delayed by a custom-built timing circuit to generate a variable pretrigger for the CO₂ laser. At time $t=200 \mu$ sec after the flashlamps have fired, the Nd:YAG laser Q-switch fires, simultaneously allowing the laser to fire. The relative arrival times of the IR and UV laser beams at the source can be observed with a photodiode detector, and adjusted as necessary with the pretrigger circuit. The Q-switch sync is used to trigger the data acquisition electronics. Thus in

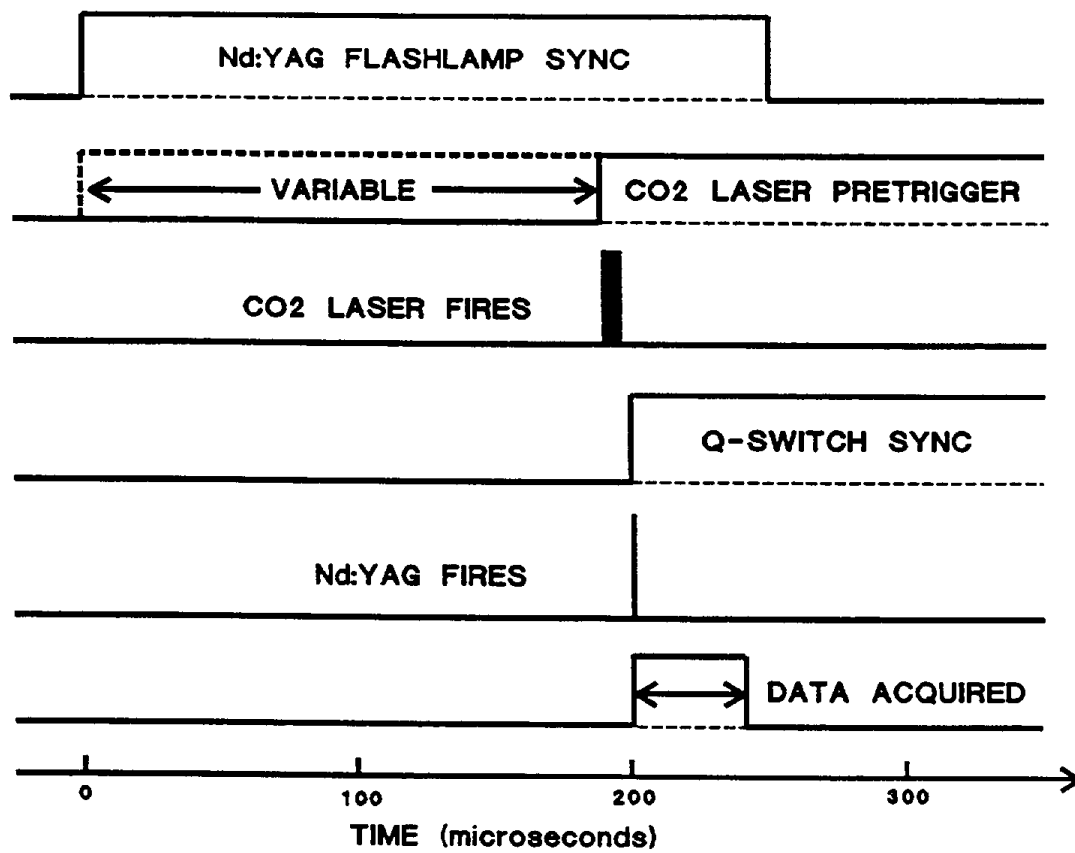


FIGURE 4. Schematic diagram of the event timing in the LDLPMS experiment.

the time-of-flight spectra, the time origin corresponds to the arrival of the UV laser pulse at the source.

2.2 Source Region Geometry

The probe design and beam path geometry within the source region, illustrated in Figure 5, are critical for the success of the two-step LDLPMS experiment. An aluminum probe tip was machined with a flattened face which is at 90° to the flight tube axis. The sample filter is attached to this face using sticky tape. The probe can be raised and lowered so that different spots on the sample can be analyzed. Electrical contact is made between the probe tip and the repeller plate so that the electrical field gradient remains uniform.

The IR beam is focussed from above into the source region, and directed onto the probe face by two intra-cavity gold-plated mirrors. The placement of these mirrors is such that the IR beam impinges at an angle of approximately 30° to the probe face. The IR laser pulse causes the generation of a thermally desorbed plume composed largely of neutral molecules, which spreads out about an axis perpendicular to the probe face. Thus the desorbed molecules have their primary velocity component along the same axis as the flight tube. This is an important consideration for optimum ion transmission and in the ultimate resolution obtained in the TOF mass spectra.

At some fixed time after the arrival of the IR pulse, the focussed UV beam is pulsed into the plume of desorbed neutrals to effect multiphoton ionization. The UV beam is perpendicular to the flight tube axis, so that the ions formed have the same spatial origin with respect to their distance from the extractor plate. The exact position of the UV beam with respect to the probe face, as well as the relative arrival times of the IR and UV beams, significantly affect the ion intensities and flight times in the recorded mass spectra. It was imperative to optimize these experimental parameters prior to routine data collection.

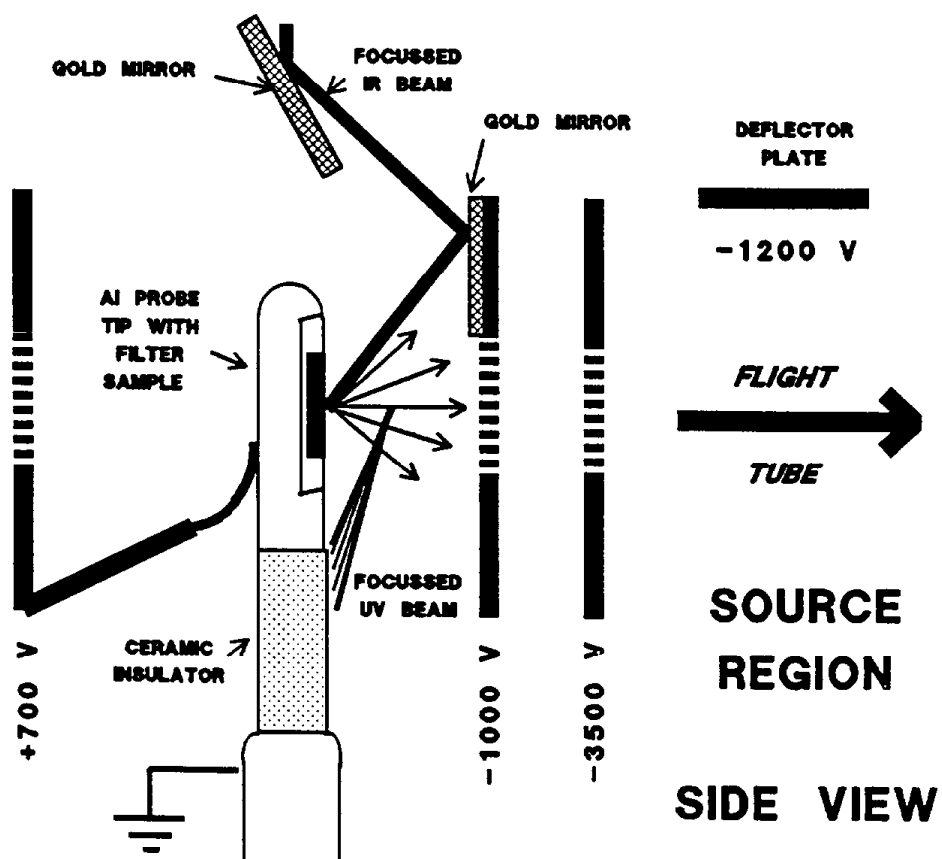


FIGURE 5. Diagram of the source region of the time-of-flight mass spectrometer, showing the beam geometries for the IR and UV lasers.

2.3 Standard PAH Compounds

PAH standard compounds were obtained from Aldrich (98 %-99 % purity) and used as received. Glass fiber air-sampling filters (Gelman Type A/E) were used as the sample substrate. Usually, a solution of the standard in CS₂ was prepared at a concentration of several mg/ml. Approximately 50 μ l of the solution was dropped by syringe onto a 1 cm² piece of the filter substrate, and allowed to air-dry. This relatively high working concentration was necessitated by the high vapor pressure of the PAH compounds. The glass fiber filter has poor retention for the PAHs alone, so that a significant portion of the sample is pumped off within minutes of insertion into the instrument. In the future, this problem may be remedied by binding the PAH to a matrix such as graphite, or by the use of a filter substrate which has a greater affinity for PAHs. Alternatively, the probe tip could be cooled with a sub-miniature thermoelectric heat pump.

2.4 Mass Calibration of LDLPMS Spectra

The raw LDLPMS spectra consist of signal intensity versus flight time. Since mass is proportional to the square of flight time in a TOF mass spectrum, the data files are stored as flight time squared and intensity data-pairs. A mass calibration for each sample run was obtained by fitting the square of flight time for the lower mass fragment ions to a second order polynomial. The precision of the fit was usually within 1%. Improved software for data collection and analysis is currently under development to allow mass calibration of spectra as they are acquired.

3. RESULTS

3.1 Optimization of the LDLPMS Method

When a pulse of IR photons of power density 10^6 - 10^7 W/cm² are incident upon a surface, a rapid increase of the surface temperature occurs within nanoseconds. Heating rates on the order of 10^8 K/sec have been measured for quartz and glass surfaces (3). At such rapid heating rates, intact molecules are desorbed before competing side reactions which lead to fragmentation can occur. As laser induced thermal desorption is initiated, a plume of desorbed molecules evolves about an axis perpendicular to the surface. At some time after the arrival of the pulse of IR photons, the photoionization laser beam interrogates the desorbed plume at a fixed distance from the surface. The flux of molecules at a fixed distance from the surface over a period of time, usually microseconds, depends on the velocity distribution of the desorbed molecules. Assuming a Boltzmann temperature distribution, the flux at a given distance will have a Maxwell-Boltzmann type distribution over time. That is, the flux will increase to a maximum value, and then decrease more slowly. Clearly, in order to optimize the ion yield, the photoionization pulse should be synchronized in time and space as close to the maximum flux of desorbed molecules as possible.

It is difficult to predict *a priori* the optimum experimental parameters which correspond to maximum ion yield. The surface heating rate depends on the thermal and optical properties of the substrate. The desorption yield will also depend on the desorption activation energy of the adsorbate. In order to optimize the relative arrival times of the desorption and photoionization beams, as well as the position of the photoionization beam with respect to the desorption surface, a substrate which closely resembles the soot samples should be used. The desorption yield from the sample should also remain constant over many IR laser pulses. It was found that graphite powder smeared onto a glass fiber air-sampling filter met these requirements. Because graphite is a highly ordered material, stable carbon clusters are formed by laser desorption. A

characteristic carbon cluster of approximate mass 200 was readily desorbed and gave a reproducible ion intensity yield for a given set of conditions.

In order to optimize the experimental parameters, the pretrigger time for the CO₂ laser was varied from 2 μ sec to 20 μ sec in 2 μ sec steps. At the same time, the position of the UV beam with respect to the probe face was varied from 0.50 mm to 2.00 mm in 0.25 mm steps. The power density of the IR beam remained constant at 10 MW/cm². The UV power was adjusted to maximize the parent ion yield without inducing fragmentation.

The time-of-flight spectra in Figure 6(a) illustrate the affect of the IR pretrigger time on ion yield for a UV beam position fixed at 1.00 mm from the probe face. The integrated intensity of major cluster ion peak, plotted as a function of IR pretrigger time in Figure 6(b), rises rapidly from 2 μ sec to 8 μ sec, peaking between pretrigger times of 8 to 10 μ sec. The ion yield then decreases more gradually. This is the type of behavior expected for a Maxwell-Boltzmann distribution of velocities.

A broad, noisy feature was observed near the origin of the LDLPMS spectra, particularly for short IR pretrigger times. Spectra collected with no photoionization beam, Figure 7, indicate that this feature is associated with the thermal desorption process. As the pretrigger time increases, the feature moves to shorter flight times and gradually moves out of the spectra at longer pretrigger times. It can be attributed to ions which are originally present in the sample, particularly sodium, or ions which are formed in the thermal desorption process via sodium or hydrogen adduct formation. These ions will have shorter apparent flight times than ions formed in the photoionization beam. It is important to note that this low intensity feature does not contribute significant intensity to the photoionization spectra, particularly for pretrigger times of 10 μ sec or more.

The influence of UV beam position for spectra collected at the same IR pretrigger time is seen in Figure 8(a). At a pretrigger time of 10 μ sec, the integrated intensity of the major cluster ion peak, plotted in Figure 8(b), decreases threefold as the photoionization beam is moved from 0.50 mm to 2.00 mm away from the probe face. The peak shape also degrades as the UV beam is moved away from the probe face,

EFFECT OF IR PRETRIGGER TIME ON ION YIELD

UV BEAM POSITION: 1.00 mm

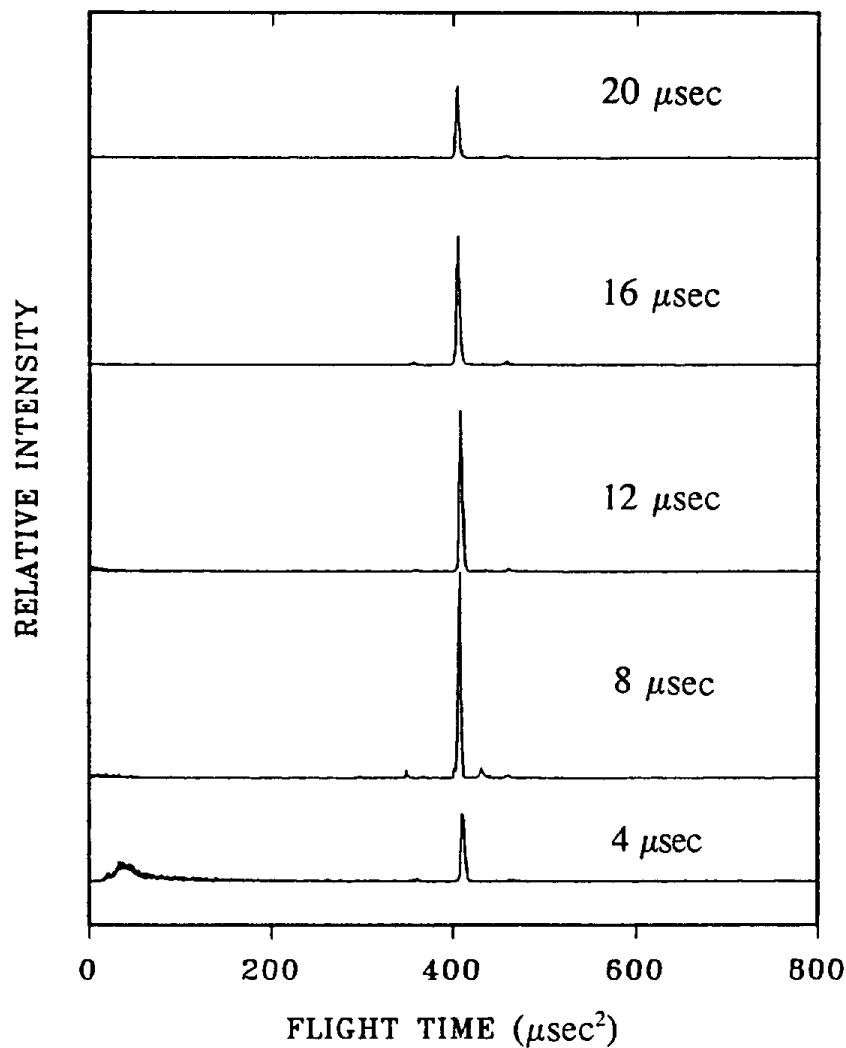


FIGURE 6(a). Time-of-flight spectra illustrating the effect of IR pretrigger time on ion yield. The UV beam position is fixed at 1.00 mm from the probe face. Sample: Graphite on Gelman glass fiber air-sampling filter.

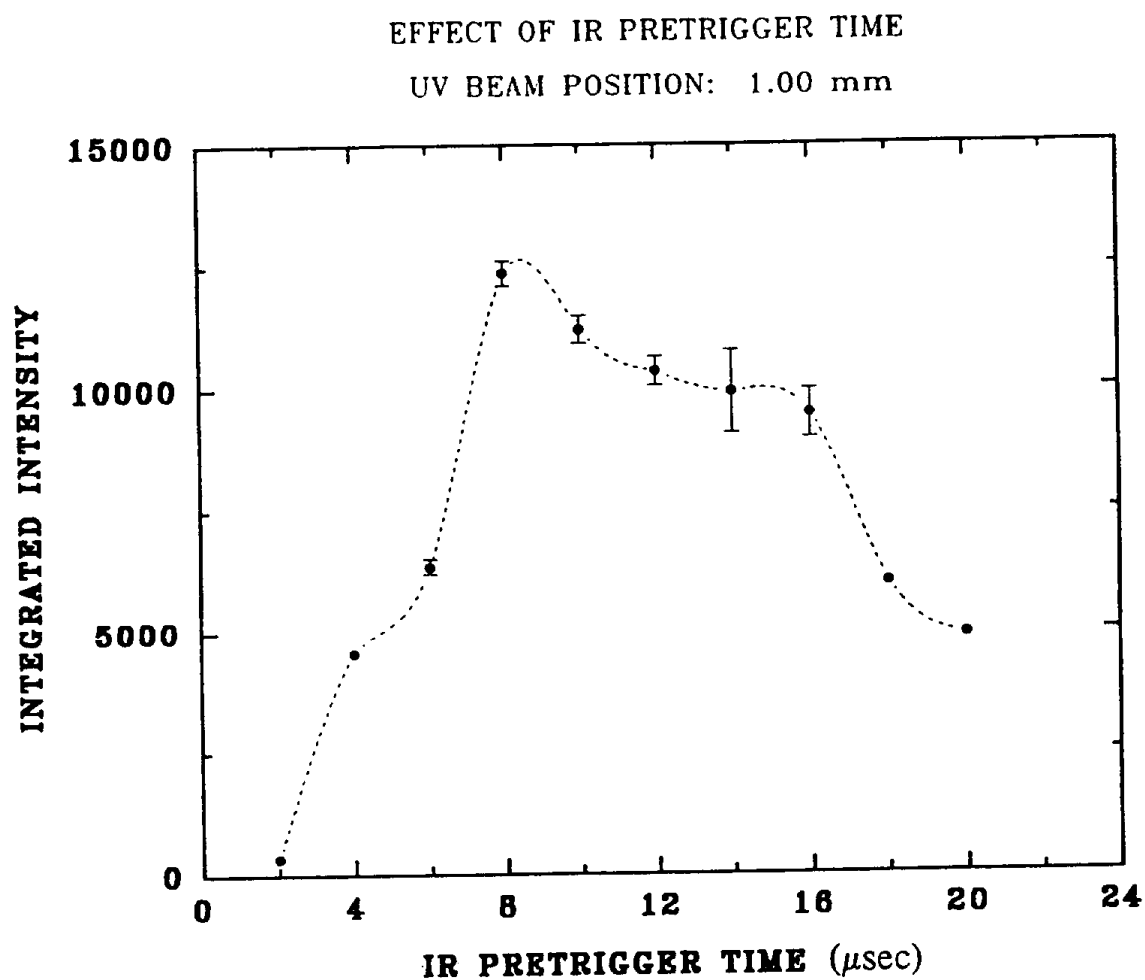


FIGURE 6(b). Effect of IR pretrigger time on integrated intensity of major cluster ion peak from graphite. UV beam position is fixed at 1.00 mm from the probe face.

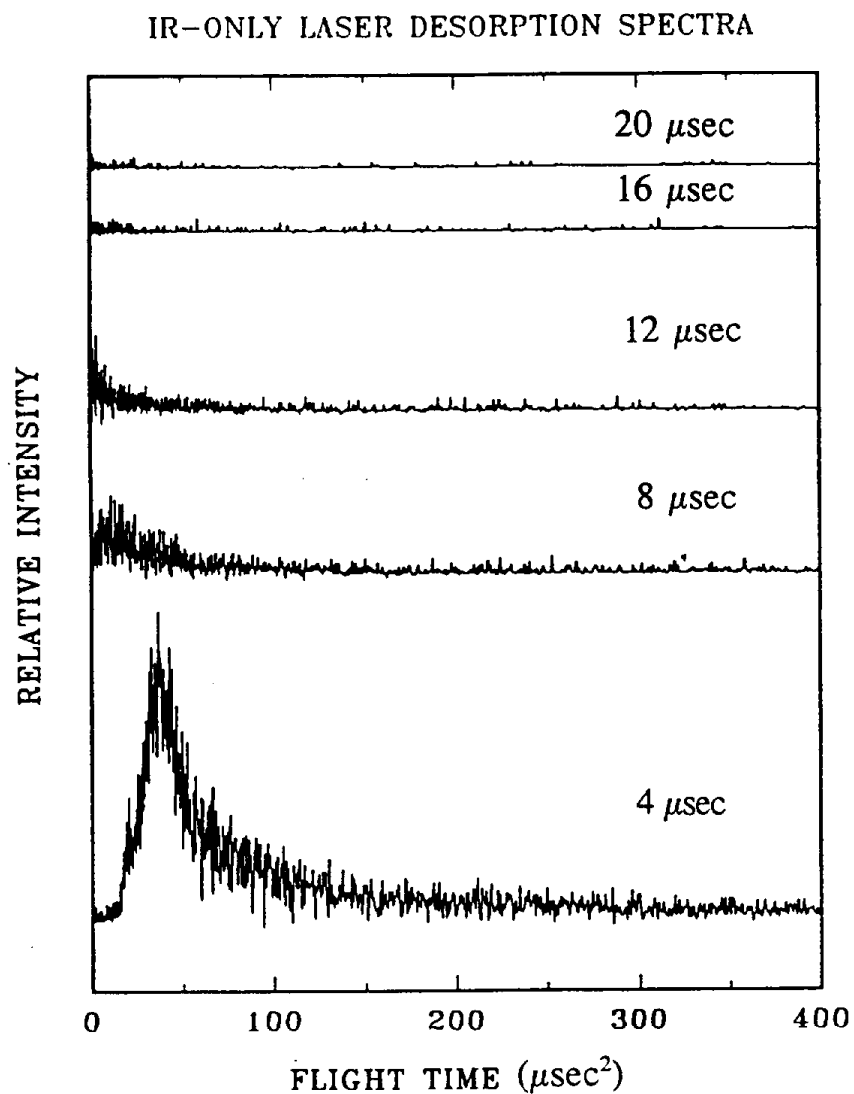


FIGURE 7. IR-only thermal desorption time-of-flight spectra obtained with no UV photoionization, showing effect of IR pretrigger time. Sample: Graphite on Gelman glass fiber air-sampling filter.

becoming noisier and asymmetric. Since ions which are formed farther away from the probe face travel a shorter distance through the potential gradient in the source region, they are not as well focussed as ions with longer flight distances.

It is also evident in examining the time-of-flight spectra in Figure 8 that the flight times of the pyrene peak are shifted as the ionization position is changed. A plot of flight time versus UV beam distance from the probe, Figure 9, shows that the flight time increases 2 μ sec from 0.50 mm to 2.00 mm. This is a significant shift in terms of mass calibration of the spectra. Ions which are formed closer to the extractor plate have longer flight times, as they do not experience as much acceleration through the potential gradient as ions formed farther away.

The results of these optimization studies emphasize the importance of maintaining a constant set of operating parameters for routine data collection. All the LDLPMS spectra collected for this report were obtained with an IR pretrigger time of 10 μ sec, and a UV beam position 1.00 mm from the probe face.

EFFECT OF UV BEAM POSITION ON ION YIELD

IR PRETRIGGER TIME: 10 μsec

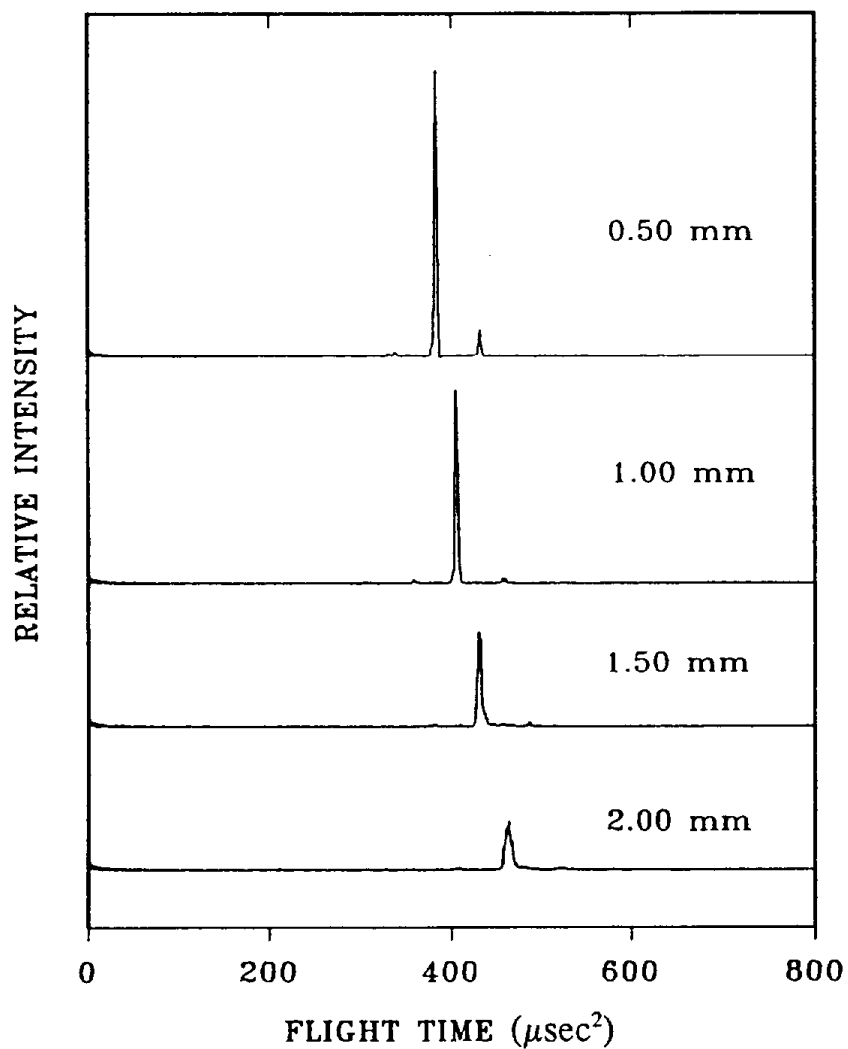


FIGURE 8(a). Time-of-flight spectra illustrating the effect of UV beam position on ion yield. IR pretrigger time is fixed at 10 μsec . Sample: Graphite on Gelman glass fiber air-sampling filter.

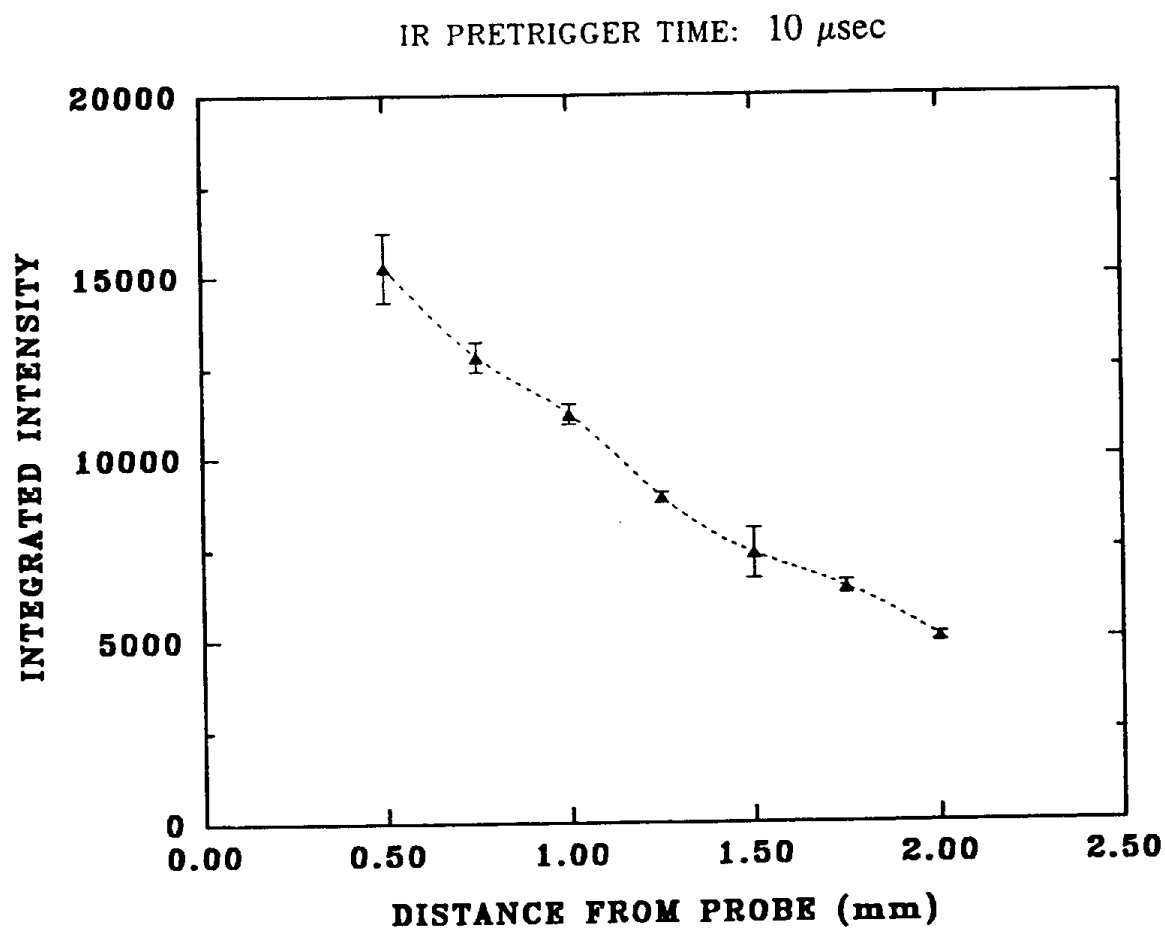


FIGURE 8(b). Effect of UV beam position on the integrated intensity of the major cluster ion peak from graphite. IR pretrigger time fixed at 10 μ sec.

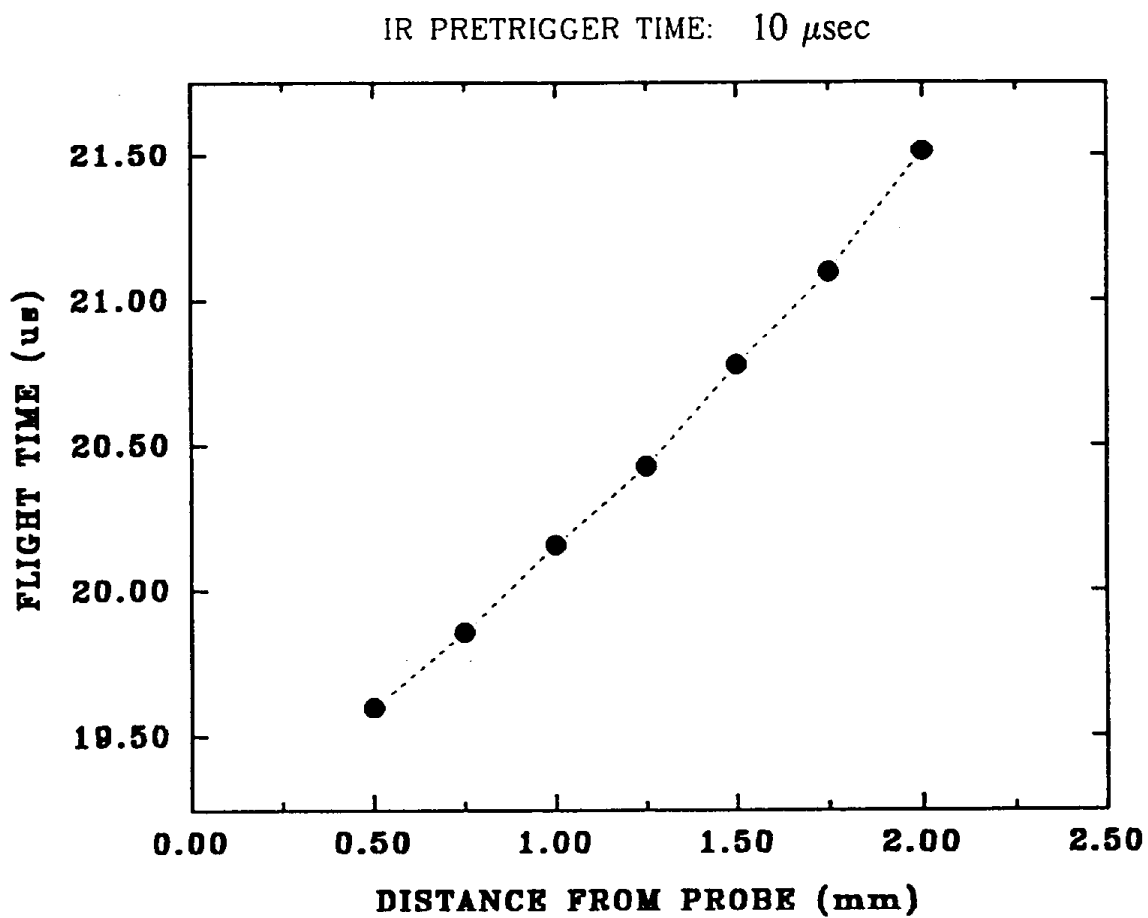


FIGURE 9. Effect of UV beam position on the flight time of the major cluster ion peak from graphite. IR pretrigger time is fixed at 10 μ sec.

3.2 LDLPMS of PAH Standards

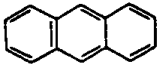
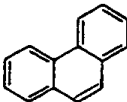
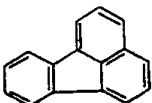
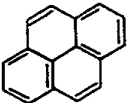
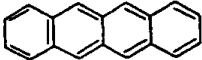
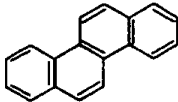
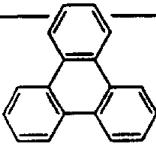
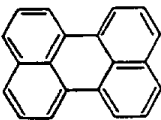
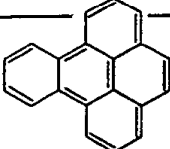
Table 1 lists the PAH standards selected for this study and some of their properties. Four different isomer pairs ranging from molecular weight 178 to 252 and ring sizes three to five were chosen. All are excellent chromophores with maximum absorptivities on the order of $10^4 \text{ L mol}^{-1} \text{ cm}^{-1}$ in the spectral region 200 nm to 300 nm. Since all of the PAHs studied have some degree of absorptivity at 266 nm, the LDLPMS spectra in both the "soft" and "hard" ionization modes were investigated at this wavelength. The ionization potentials lie between 7 and 8 eV, so that two photon ionization with 266 nm radiation (equivalent to 9.32 eV) is possible for all these compounds. The LDLPMS spectra are collected in Appendix I.

In the "soft" ionization mode, the parent molecular ion peak, M^+ , was the dominant feature in the LDLPMS spectra for all the PAHs tested. Figures 10 and 11 illustrate the 266 nm photoionization spectra of the isomer pair anthracene and phenanthrene, respectively. Little or no fragmentation was observed at low UV power. In phenanthrene, however, a peak approximately 12 mass units higher than the parent peak appears. This was also observed in pyrene, triphenylene, and perylene with 266 nm radiation. This may be evidence of single carbon unit photoattachment.

When the UV power was increased to induce "hard" ionization, the resulting fragmentation patterns were dominated by the low mass carbon fragments corresponding to C through C_6H_x in all PAHs studied. These fragment peaks are shown in more detail for anthracene and phenanthrene in Figure 12. In the anthracene spectrum, the peaks are beautifully resolved, showing unit mass resolution up to C_7 . In contrast, the peaks are poorly resolved in the phenanthrene spectrum. This poor resolution was also observed for fluoranthene.

Lower intensity fragment peaks at intermediate mass corresponding to the loss of one or two acetylene units (C_2H_2) were also observed in the LDLPMS spectra of all the PAHs examined. These peaks generally were not as well resolved as the carbon fragments. Figure 13 illustrates a series of photoionization spectra for pyrene obtained

TABLE 1. PROPERTIES OF SELECTED POLYCYCLIC AROMATIC HYDROCARBONS

COMPOUND	MOLECULAR FORMULA	MOLECULAR WEIGHT	IONIZATION POTENTIAL (eV)	STRUCTURE
ANTHRACENE	$C_{14}H_{10}$	178	7.41	
PHENANTHRENE	$C_{14}H_{10}$	178	7.86	
FLUORANTHENE	$C_{16}H_{10}$	202	7.72	
PYRENE	$C_{16}H_{10}$	202	7.80	
NAPHTHACENE	$C_{18}H_{12}$	228	6.97	
CHRYSENE	$C_{18}H_{12}$	228	7.59	
TRIPHENYLENE	$C_{18}H_{12}$	228	7.88	
PERYLENE	$C_{20}H_{12}$	252	7.03	
BENZO[e]PYRENE	$C_{20}H_{12}$	252	7.61	

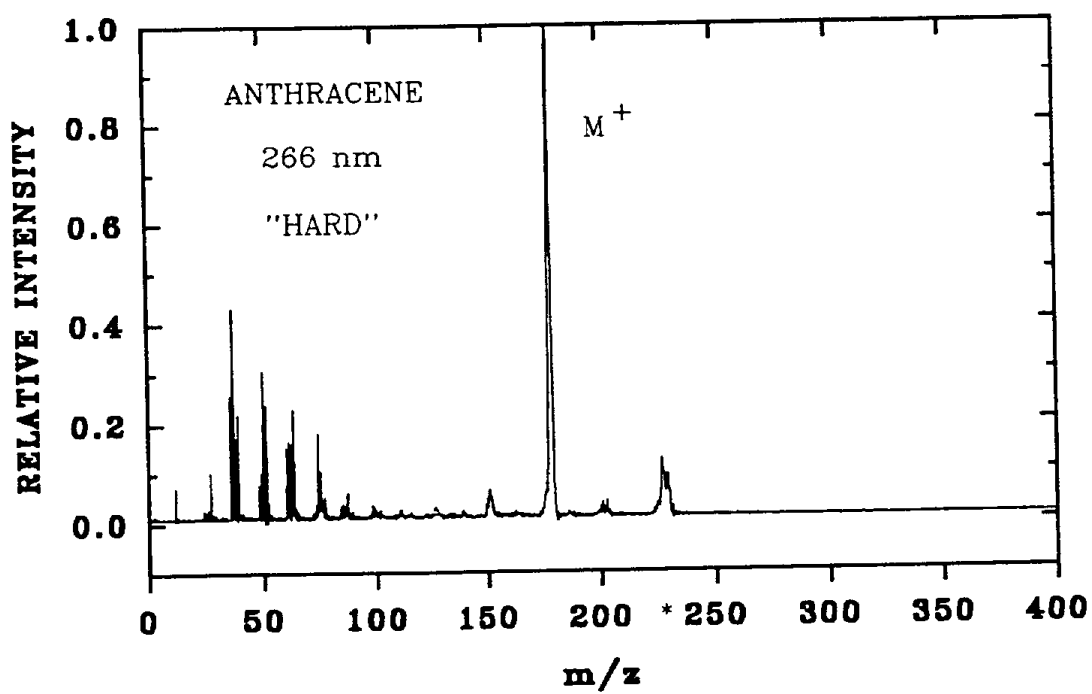
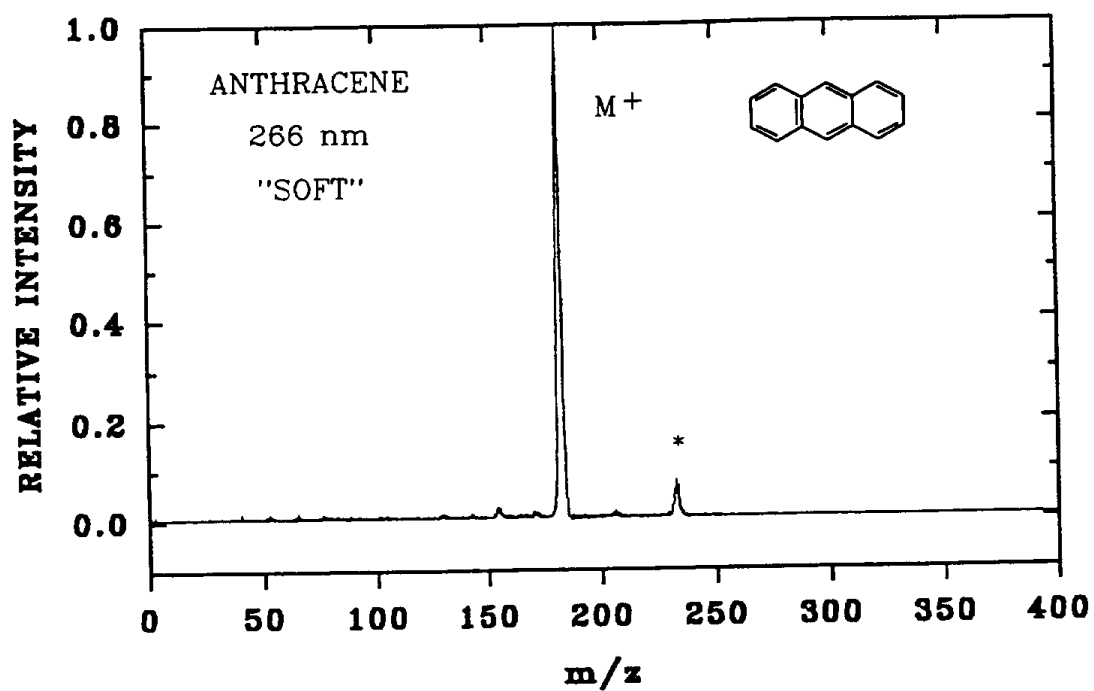


FIGURE 10. LDLPMS spectra of anthracene obtained at 266 nm. (* = contaminant)

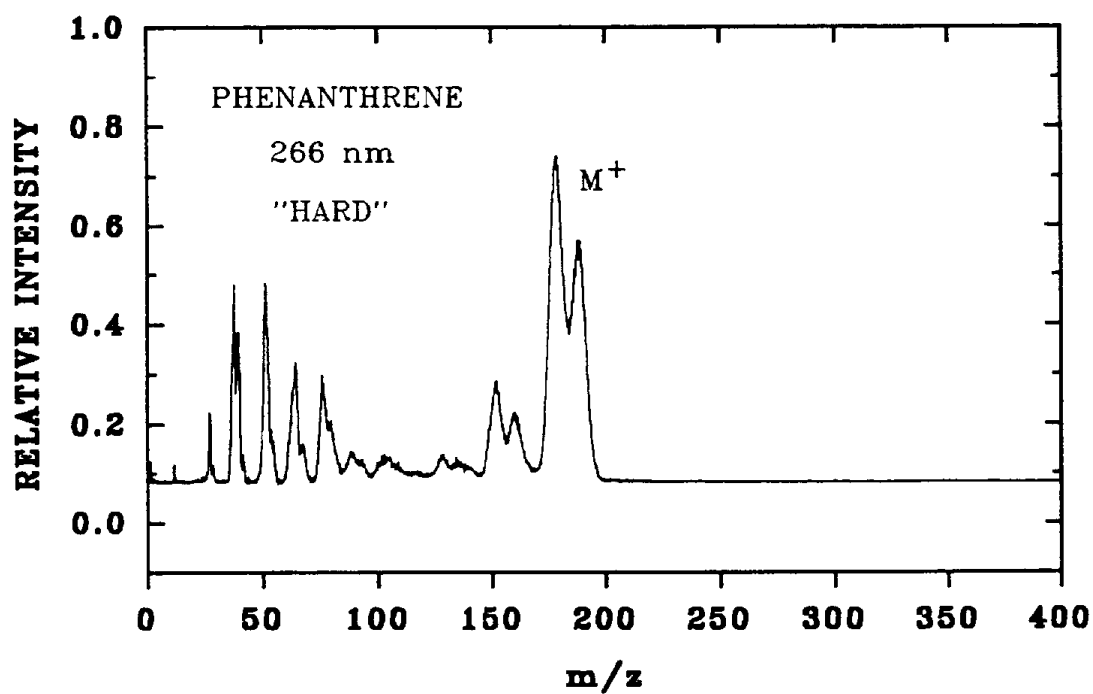
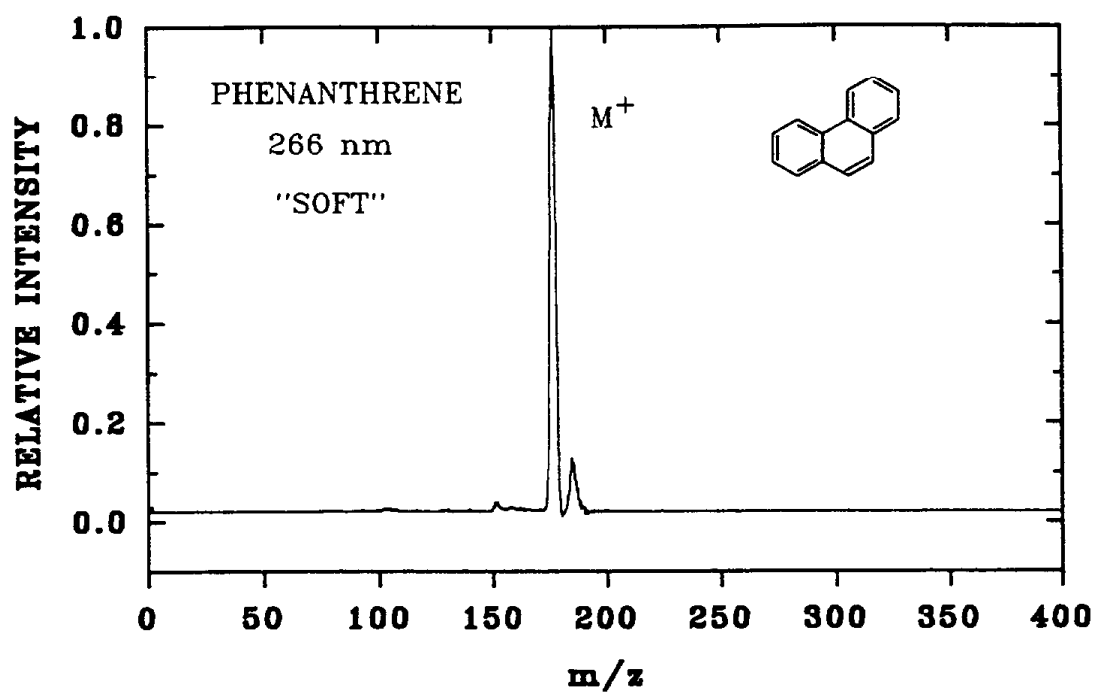


FIGURE 11. LDLPMS spectra of phenanthrene obtained at 266 nm.

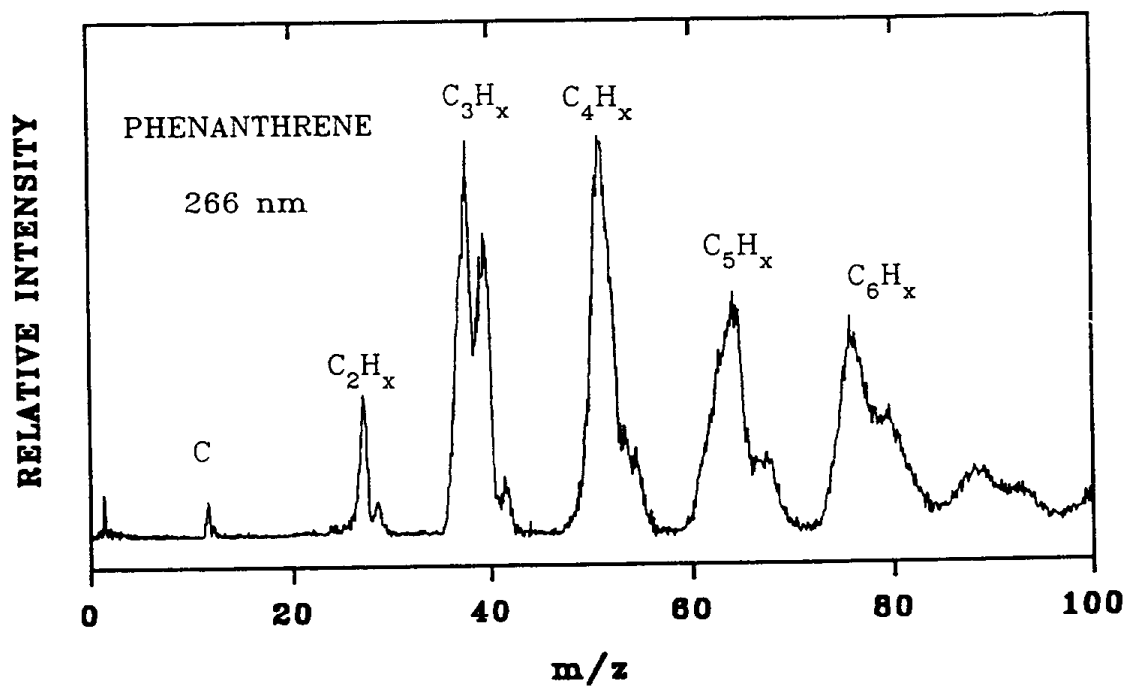
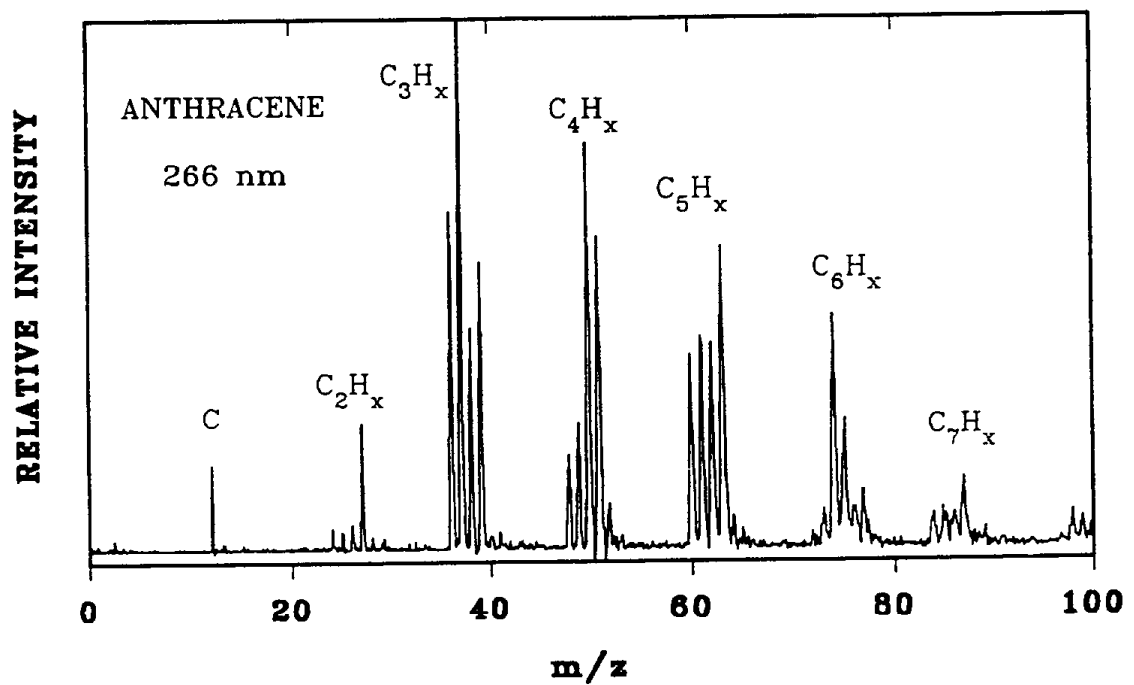


FIGURE 12. Detail of LDLPMS spectra of anthracene and phenanthrene obtained at 266 nm, showing low mass carbon fragment patterns.

with increasing UV power. Note that the intensities of the fragment ion peaks at m/z 178 and 152, relative to the parent ion peak intensity, do not change significantly after the onset of fragmentation. Rather, increasing UV power causes the intensities of the low mass carbon fragments to increase dramatically. At the same time, the parent ion peak loses intensity. At very high UV power, the parent ion peak is broadened and noisy. This may be caused by space charge effects in the ionization volume. As the number of positive ions formed is increased, Coulombic repulsion causes spatial broadening.

It is interesting to compare the photoinduced fragmentation with that produced by electron ionization (EI) techniques. In 70 eV EI spectra of PAHs, fragmentation patterns corresponding to the consecutive loss of acetylene units are observed (4). Usually the peaks corresponding to the loss of one or two acetylene units are the most intense fragment peaks. The lower mass carbon fragment peaks have little or no intensity. The opposite intensity pattern is observed in the photoionization spectra. In addition, a peak corresponding to the doubly charged molecular ion, M^{2+} , is usually observed in EI spectra, but is not observed in the photoionization spectra. This is not surprising, as the second ionization potentials for the PAHs are on the order of 20 eV (5).

Some preliminary work has been done in order to access the degree of selectivity which may be achieved by changing the UV wavelength. LDLPMS spectra at 299 nm have been obtained for most of the standards, and are included in Appendix I. Two photons of 299 nm radiation correspond to an energy of 8.29 eV, so that all of the PAHs studied can undergo two-photon ionization at this wavelength. However, not all of the PAHs studied have electronic states which overlap 299 nm radiation. This effect can be seen in the 299 nm LDLPMS spectra of anthracene and phenanthrene, shown in Figure 14. An intense molecular ion peak is observed in the anthracene spectrum, as well as a small photoattachment peak approximately 12 mass units higher. The appearance of photoattachment peaks was observed to varying extent for all the PAHs. Phenanthrene is an example of a compound which has poor electronic overlap at 299 nm. The parent molecular ion peak is weak, there are multiple photoattachment peaks, and the spectrum is very noisy. Of the PAHs studied, only anthracene, pyrene, and benzo[e]pyrene yielded

LDLPMS OF PYRENE @ 266 nm

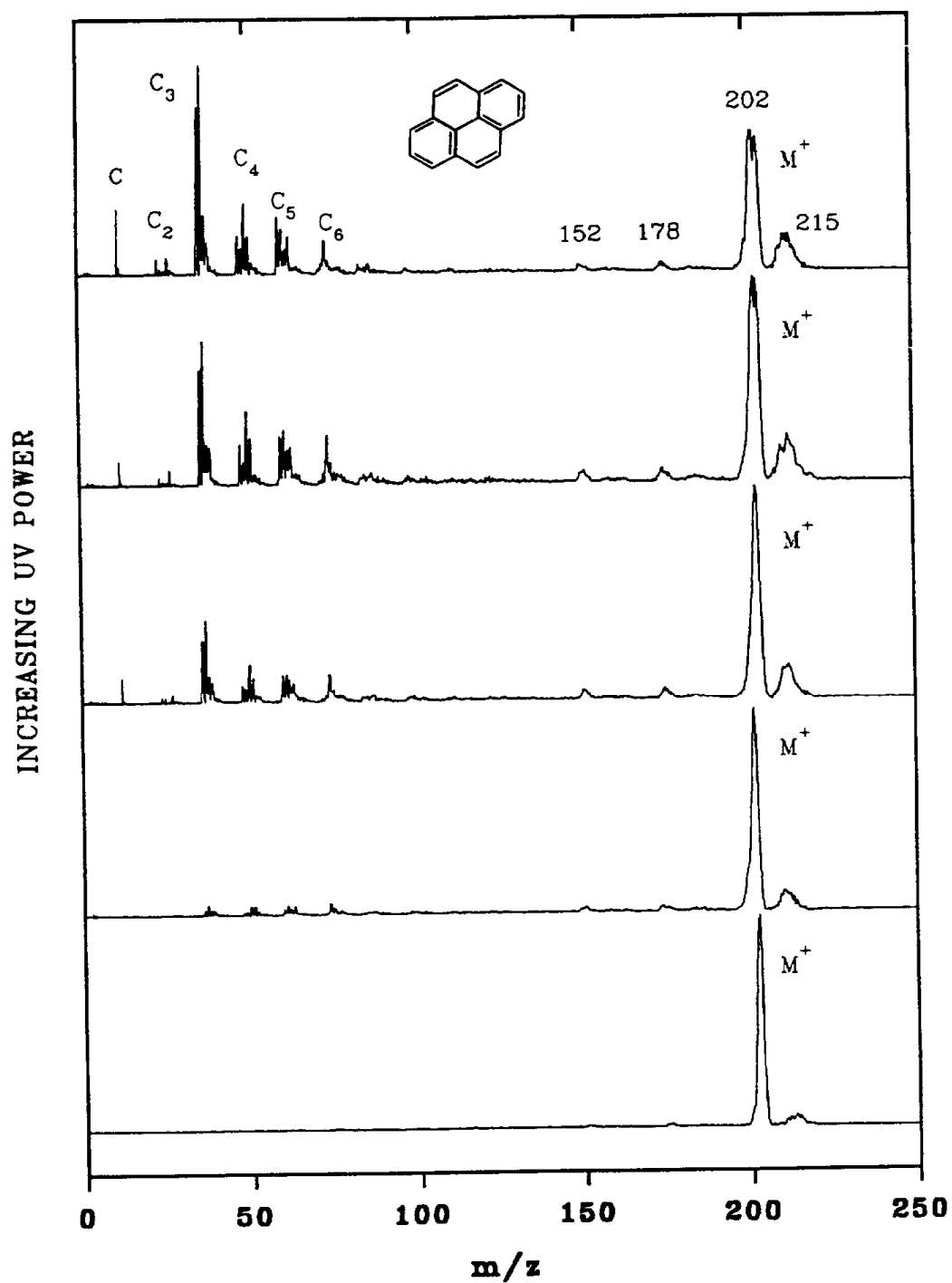


FIGURE 13. Effect of increasing 266 nm UV laser power on the LDLPMS spectra of pyrene. Each spectrum is normalized to the most intense peak.

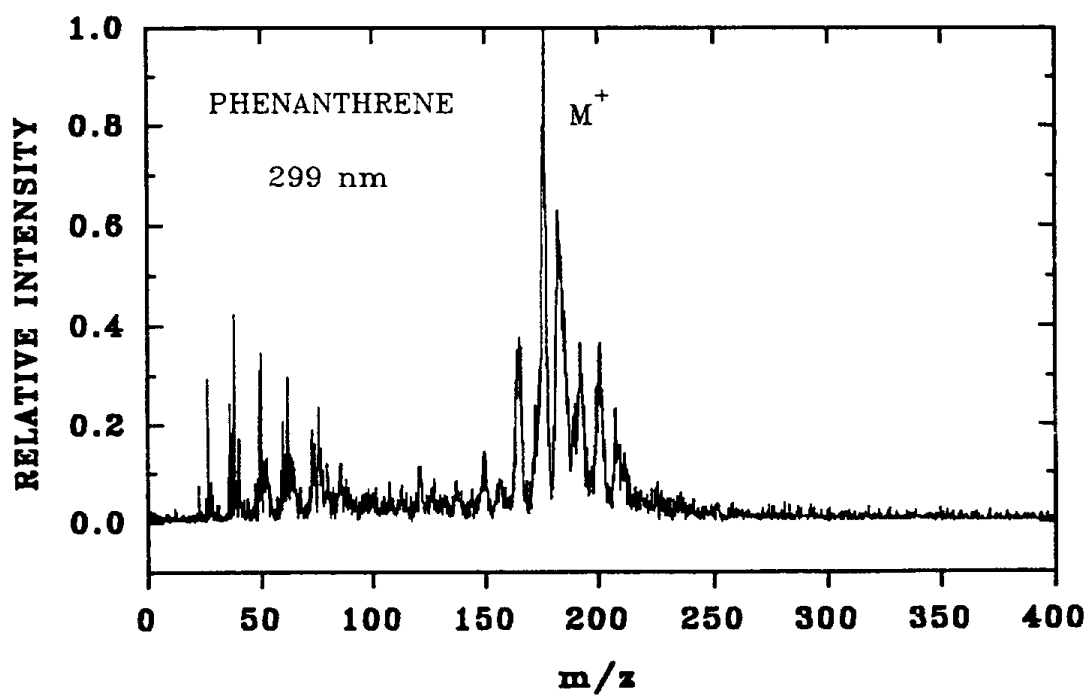
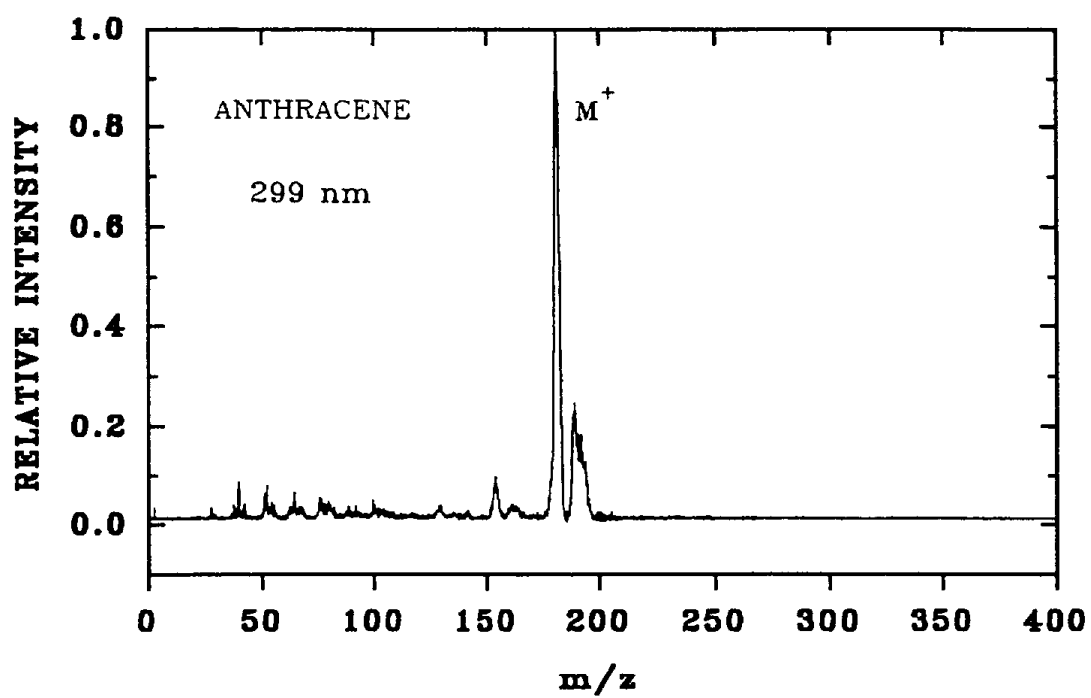


FIGURE 14. LDLPMS spectra of anthracene and phenanthrene obtained at 299 nm.

intense parent molecular ion peaks at 299 nm. The fragmentation patterns observed were similar to those in the 266 nm photoionization spectra.

The mechanism of multiphoton dissociation for large polyatomic molecules is not well understood, and it is beyond the scope of this report to speculate on the processes which give rise to the observed fragmentation patterns. However, several conclusions can be reached with regard to the present application, namely, screening for the presence of PAH compounds in soot samples:

- (i) "Soft" photoionization at 266 nm produces intense molecular ion peaks in all the PAHs studied. Thus, 266 nm photoionization is a good choice for the purpose of detecting the presence of PAHs in soot samples. However, little or no selectivity can be achieved since almost all PAHs are good chromophores at 266 nm.
- (ii) "Hard" photoionization at 266 nm produces fragmentation patterns dominated by low mass carbon fragments. The spectra contain little useful isomer-specific information, as all the PAHs dissociate by the consecutive loss of acetylene units. Some information may be gleaned from close inspection of the low mass carbon peaks, for example anthracene versus phenanthrene, but this would be of little use in the analysis of a mixture of PAH compounds.
- (iii) The preliminary results obtained with photoionization at 299 nm indicate that some degree of wavelength selectivity which would allow isomer-specific analysis may be possible. However, much more data needs to be collected and evaluated in future work to establish analytical protocols for particular PAHs.

It should be noted that the LDLPMS spectra collected to date have been obtained in the positive ion mode. The negative ion spectra may also contain valuable information, particularly for PAHs which have electronegative substituents such as halogen or nitro groups.

3.3 LDLPMS of Chlorinated Anthracene Isomers

In a preliminary study of chlorinated PAHs, two mono-substituted chloro-anthracene isomers were analyzed. Figures 15 and 16 illustrate the LDLPMS spectra of 1-chloro-anthracene and 2-chloro-anthracene, respectively, obtained with photoionization at 266 nm. Surprisingly, intense parent molecular ion peaks at m/z 213 were observed for both isomers. In the "soft" ionization spectra, a peak corresponding to the loss of chlorine at m/z 178 is always observed. As the UV power is increased, peaks corresponding to the loss of acetylene from anthracene are observed at m/z 152 and 128. A peak corresponding to loss of acetylene from the chlorinated parent is also observed at m/z 202. Comparison of the low mass carbon fragment peaks in the chlorinated and non-chlorinated anthracene molecules indicates Cl^+ is not present in the chlorinated spectra. This is not surprising, as chloride is a strongly electronegative species and would not be expected to form a positive ion under the conditions of this experiment.

These preliminary results for the MPI of monochlorinated molecules indicate that the technique may be directly applicable to the analysis of chlorinated dibenzo-*p*-dioxins (CDDs) and dibenzofurans (CDFs). However, as the degree of chlorine substitution increases, the ionization potential of the molecule also increases. The probability of forming a positive molecular ion without fragmentation will correspondingly decrease. The polychlorinated molecules would have higher electron affinities, so that examination of negative ion spectra may yield the best method for screening for chlorinated PAH molecules.

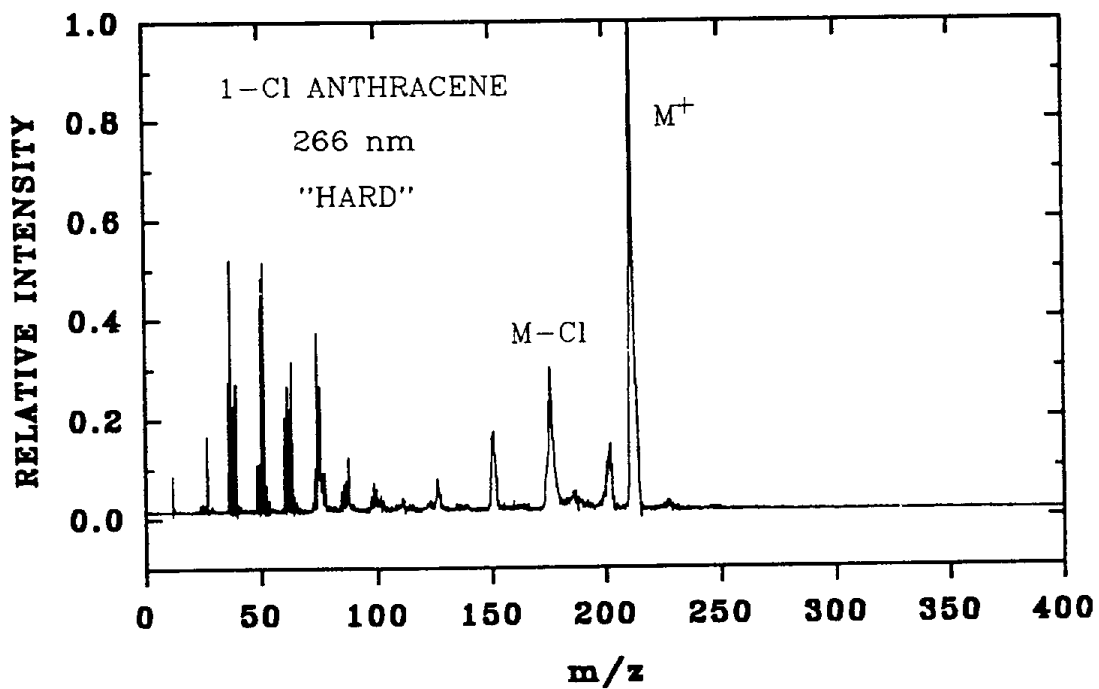
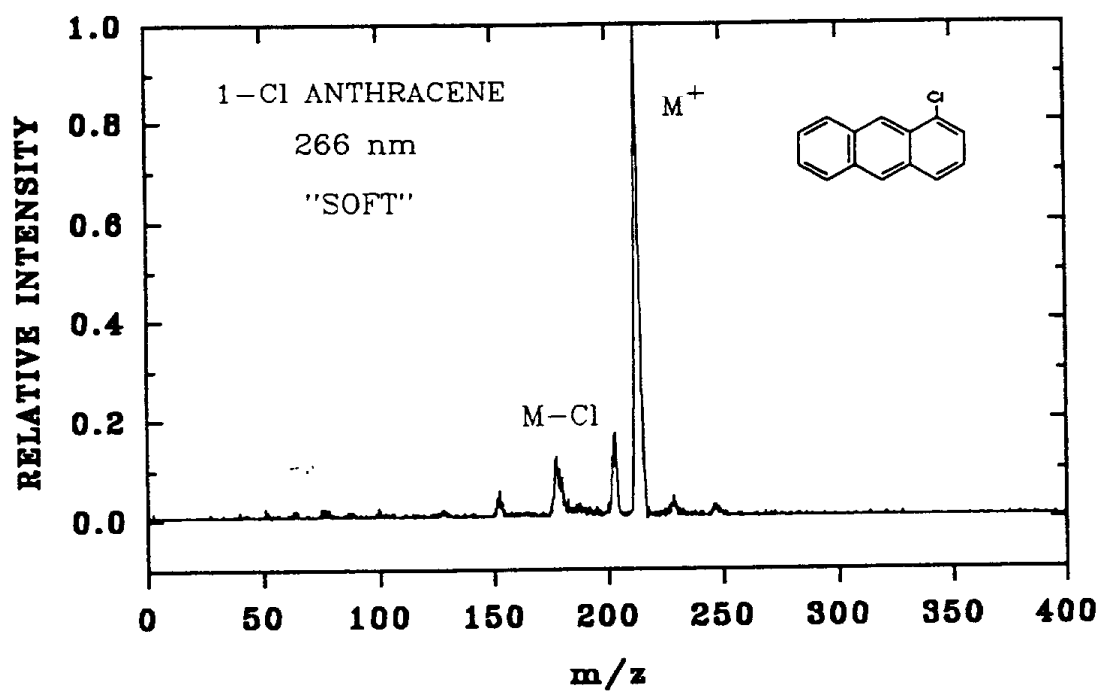


FIGURE 15. LDLPMS spectra of 1-chloro-anthracene obtained at 266 nm.

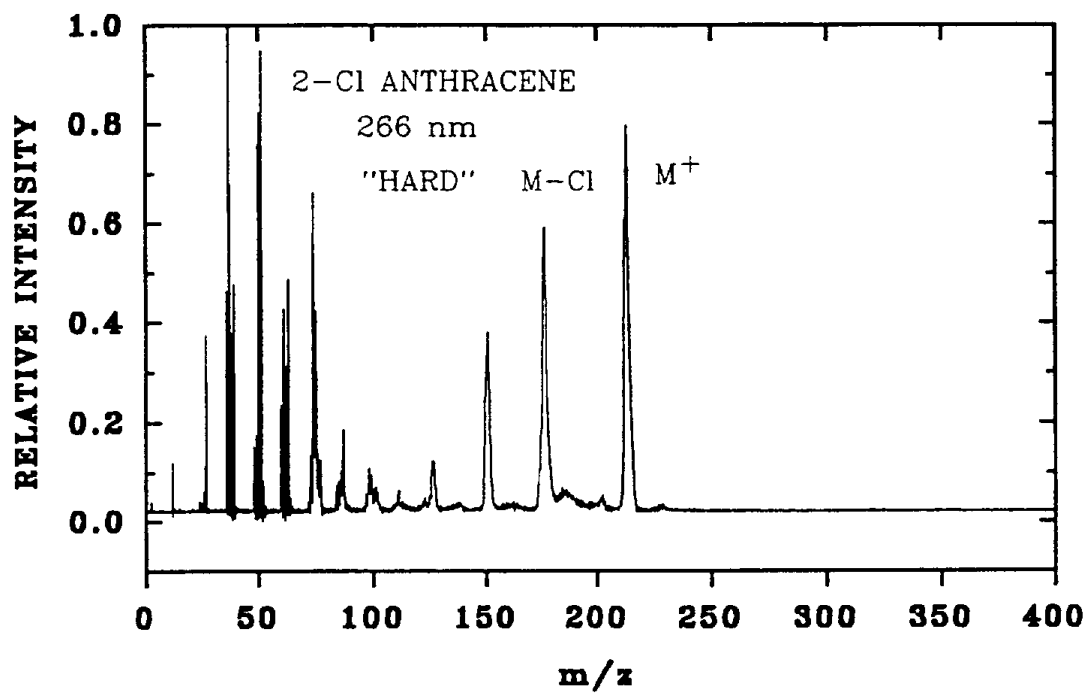
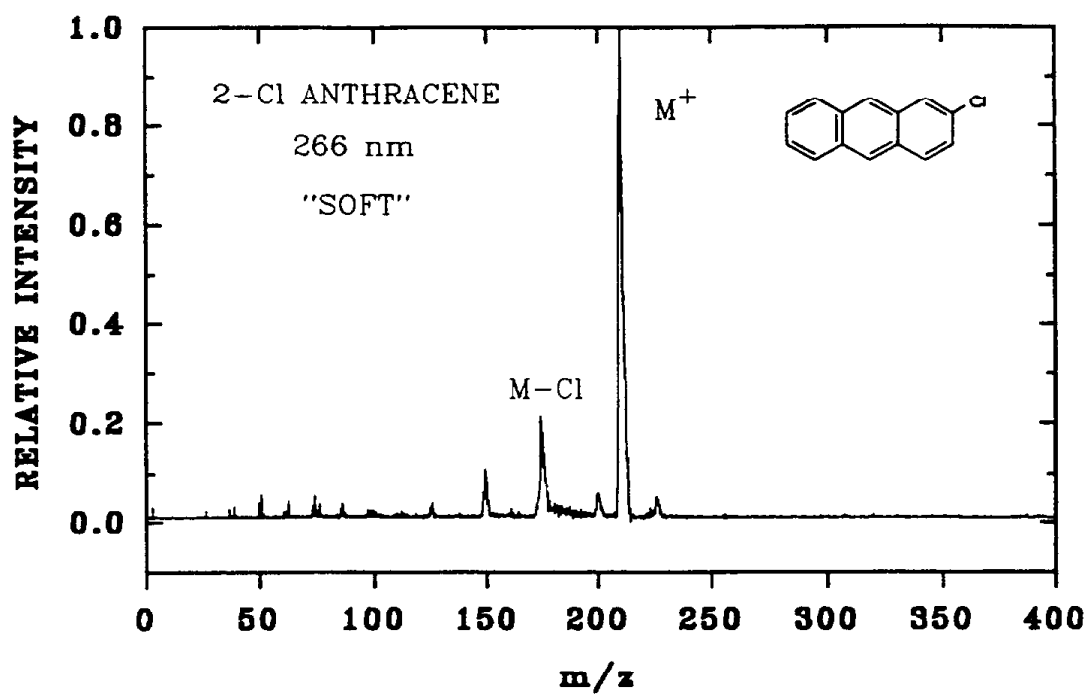


FIGURE 16. LDLPMS spectra of 2-chloro-anthracene obtained at 266 nm.

3.4 LDLPMS of Rice Soot Samples

Two rice soot samples collected on Gelman glass fiber air-sampling filters were provided by Dr. B. Jenkins and analyzed by LDLPMS as received. Figure 17 illustrates two spectra obtained with photoionization at 266 nm. The major feature of the "soft" ionization spectrum is an intense peak at m/z 202($\pm 1\%$), which corresponds to a condensed four-ring PAH such as fluoranthene or pyrene. Less intense peaks at m/z 178($\pm 1\%$) and m/z 228($\pm 1\%$) also appear, corresponding to three-ring and four-ring PAHs respectively. Smaller peaks at m/z 152, 160, 186, 192, 215, 252 and 278 are also present. When the UV power was increased to induce fragmentation, the most intense fragments were the low mass carbon fragments. These fragmentation patterns are shown in more detail in Figure 18, and are typical of those observed at 266 nm for most of the PAH standards studied.

The LDLPMS spectra obtained with photoionization at 299 nm, Figure 19, also revealed the presence of several PAHs in the rice soot. The overall intensity of the 299 nm spectra was lower than at 266 nm, as can be seen by comparing the baseline noise levels. However, as in the 266 nm spectra, the peak at m/z 202($\pm 1\%$) was usually the most intense feature. Three less intense peaks differing by one carbon unit each are observed at higher mass. The low mass carbon fragments are poorly defined; again, this was frequently observed in the 299 nm spectra of the PAH standards.

The effect of IR desorption power on the LDLPMS spectra was investigated. Figure 20 illustrates a series of spectra obtained at 266 nm with varying IR desorption power. There is a twofold increase in ion yield when the desorption power is increased from 1 MW/cm² to 5 MW/cm². The level of noise in the spectra increases also, particularly at short flight times. As the IR-only spectrum indicates, this background noise originates from the desorption process.

Exhaustive sampling of the same spot on the sample filter leads to very noisy spectra such as that shown in Figure 21. It appears that the morphology of the particulate matrix may be altered with lengthy IR irradiation, becoming looser and breaking down

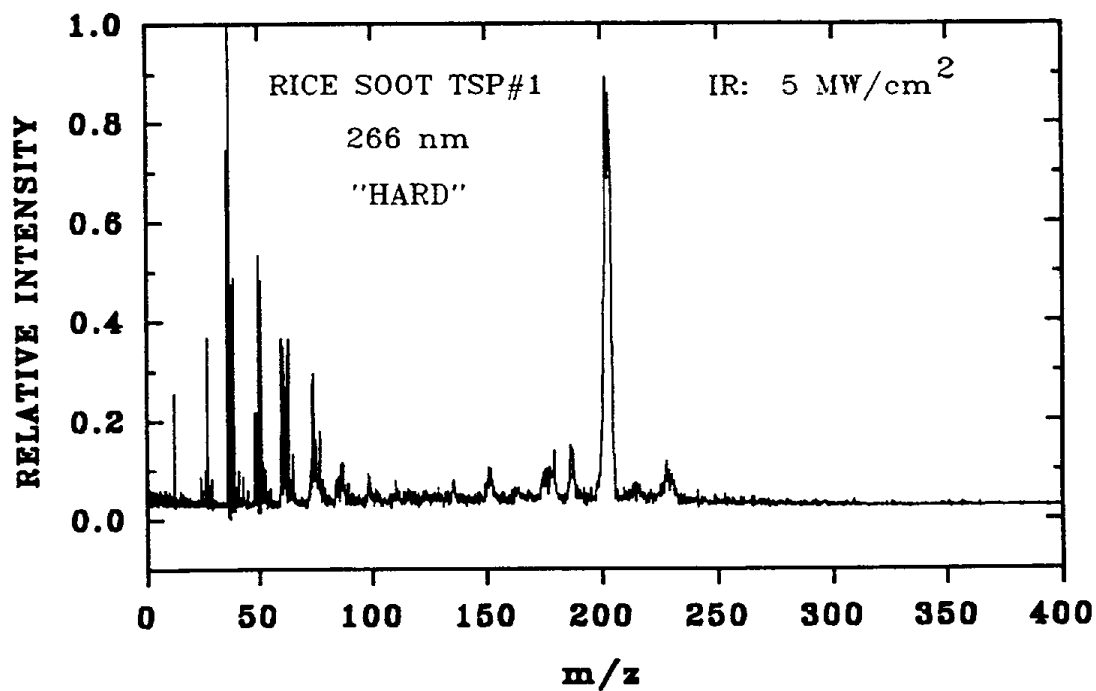
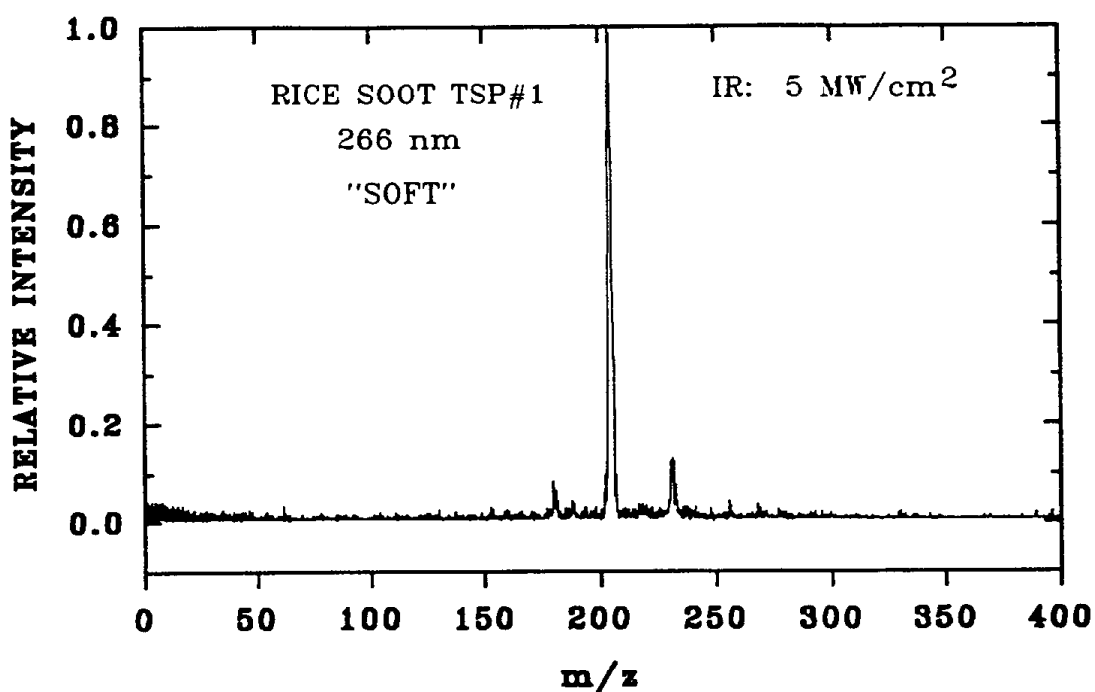


FIGURE 17. LDLPMS spectra of rice soot on air-sampling filter obtained at 266 nm.

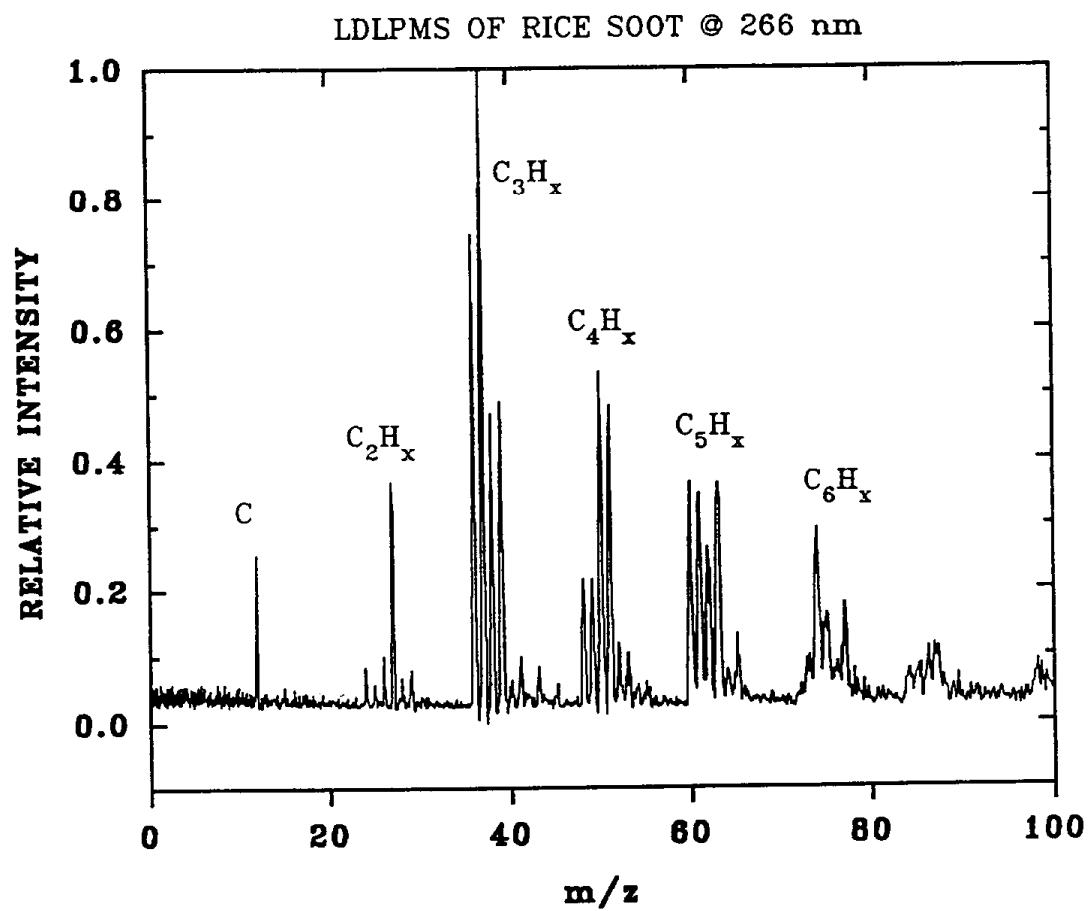


FIGURE 18. Detail of LDLPMS spectrum of rice soot showing low mass carbon fragment pattern.

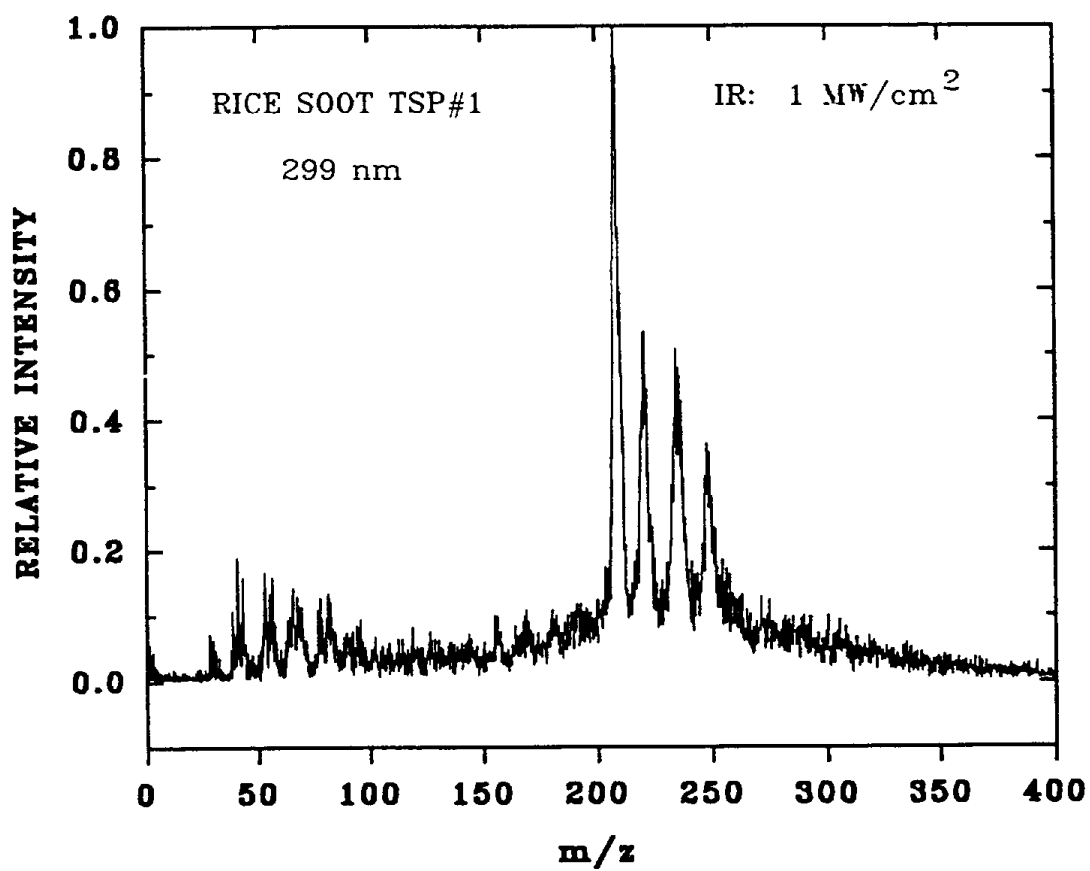


FIGURE 19. LDLPMS spectrum of rice soot on air-sampling filter obtained at 299 nm.

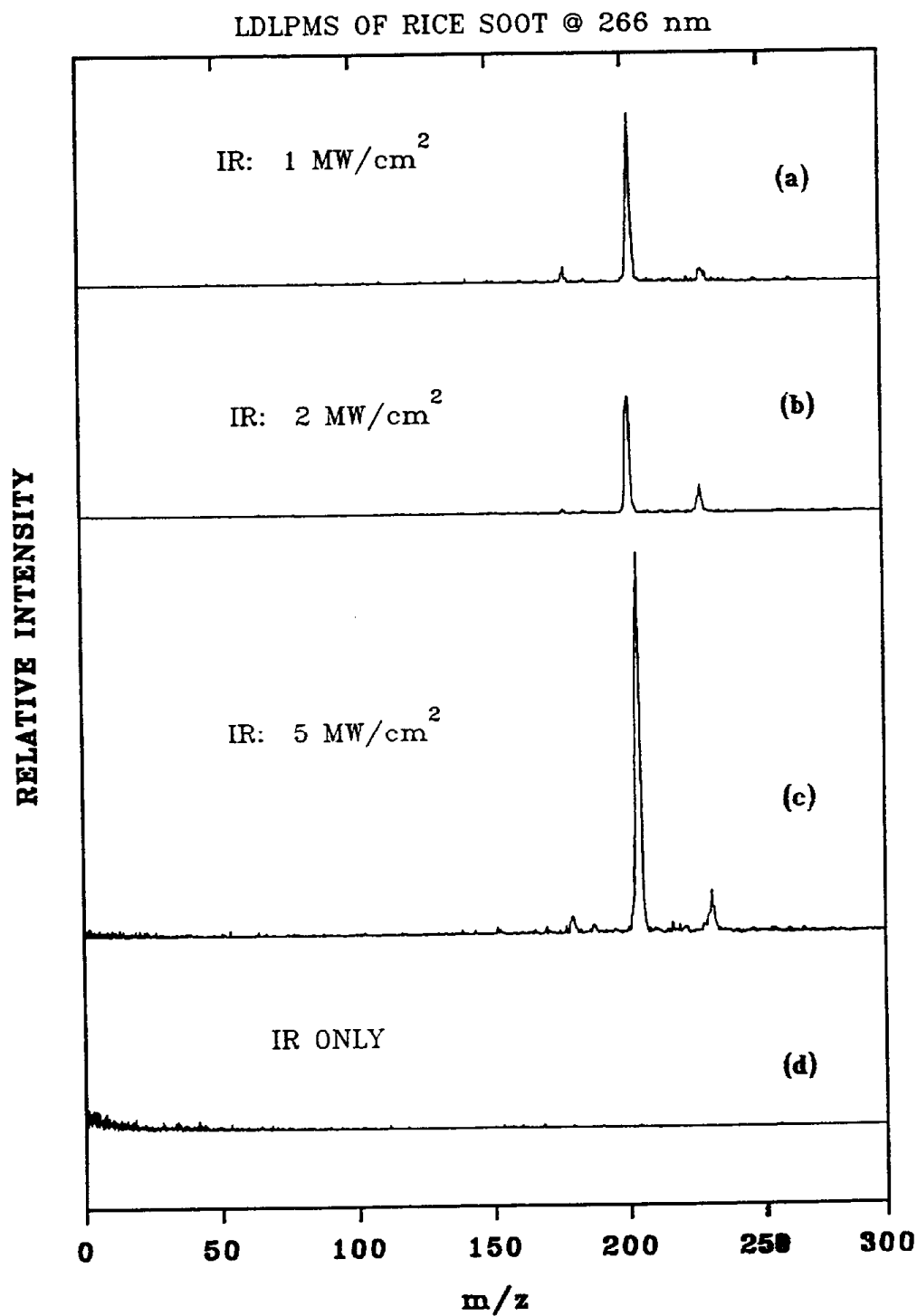


FIGURE 20. Effect of IR laser power on the LDLPMS spectra of rice soot obtained at 266 nm. (a) 1 MW/cm² (b) 2 MW/cm² (c) 5 MW/cm² (d) 5 MW/cm², no UV photoionization. Spectra are normalized to the 5 MW/cm² spectrum.

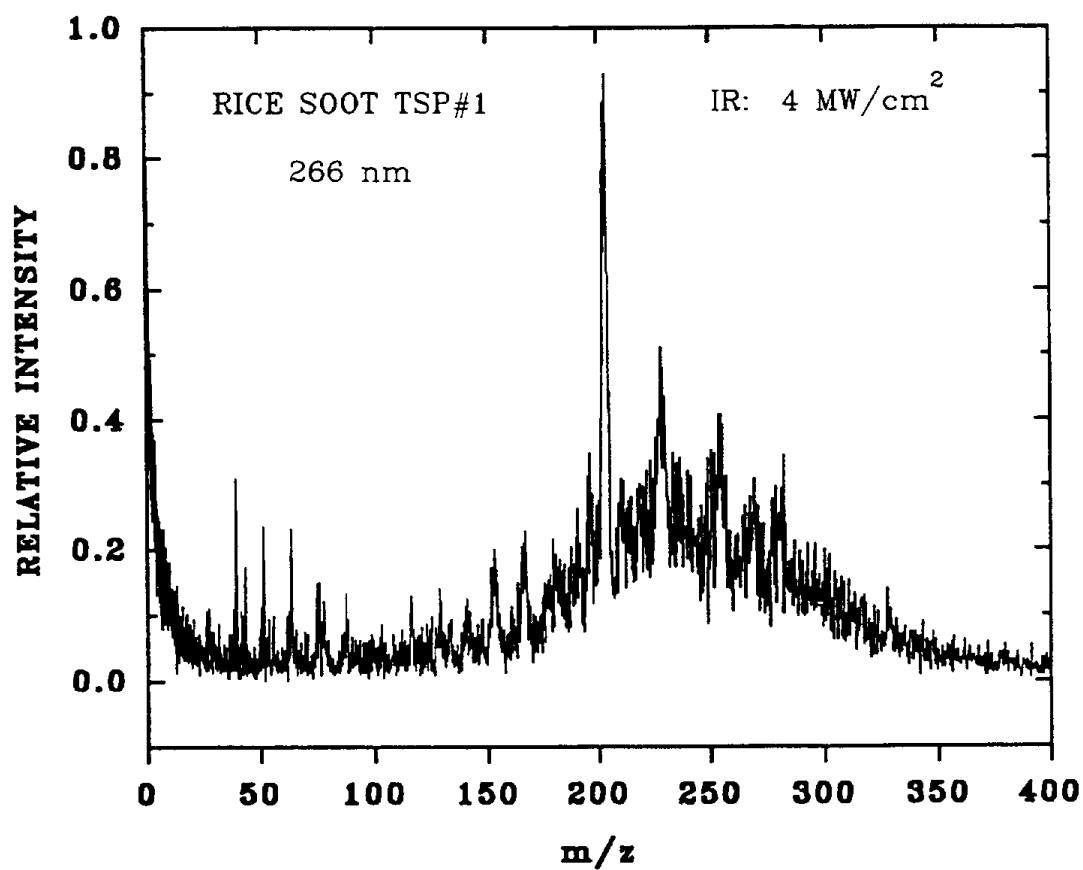


FIGURE 21. LDLPMS spectrum of rice soot on air-sampling filter obtained at 266 nm after exhaustive sampling.

into smaller particles which contribute to the background noise. This is an aspect of the LDLPMS experiment which may bear further examination.

A portion of one of the rice soot sample filters was extracted with CH_2Cl_2 and the extract was analyzed by conventional low resolution GC/MS. The results, which are included in Appendix II, indicated the presence of many PAHs in the mass range 128 to 282. Fluorene, phenanthrene, fluoranthene, and chrysene were identified by their characteristic retention times. The concentration of the PAHs was estimated to be 10-20 ng/sample. This is well below the low resolution limit for ARB Method 429 determination of PAHs, and is approaching the high resolution limit. Thus it appears that detection range of the LDLPMS method will allow screening of PAHs to well within the low resolution target detection limit. Further work is planned to ascertain the quantitative aspects of the LDLPMS method.

4.0 CONCLUSIONS

The instrumentation for the LDLPMS experiment has been designed and constructed around a custom-built TOF mass spectrometer. The LDLPMS spectra of several PAH standards have been obtained at 266 nm in both the "soft" and "hard" ionization modes. The ability of LDLPMS to screen for the presence of PAHs to within low resolution target limits in as-received rice soot samples has been demonstrated. In the future, the application of the LDLPMS method to additional types of soot and fly-ash from source and ambient aerosol samples should be examined.

Analysis of standard PAH compounds has shown that photoionization at 266 nm yields intense parent ion peaks which allows compound identification via molecular weight determination. Strong parent molecular ion peaks were also observed for two mono-chlorinated anthracene isomers. The absence of small chlorinated fragments in the positive ion spectra suggests negative ion spectra may be more valuable in the analysis of chlorinated PAH compounds such as dioxins and furans. Nitro-PAHs may also be better characterized in the negative ion mode.

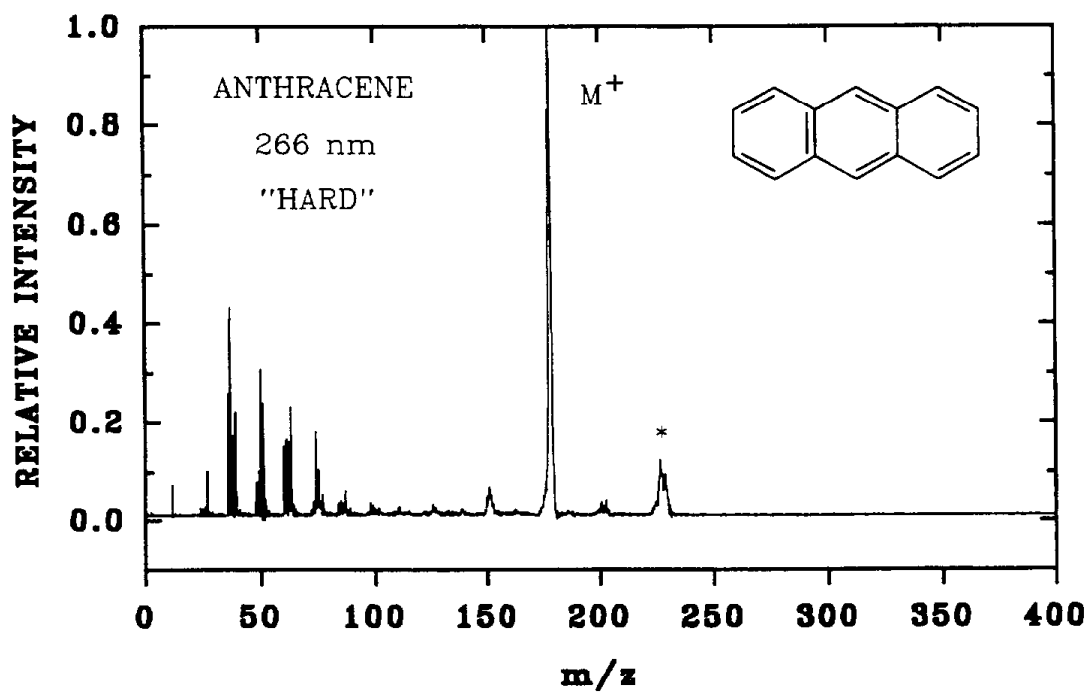
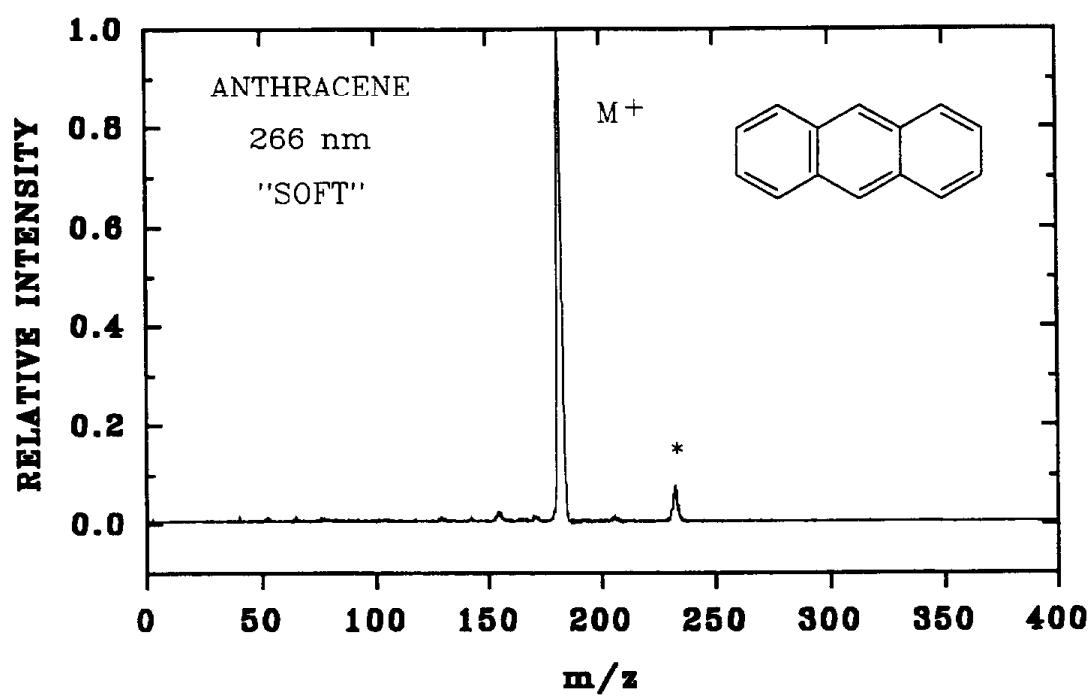
Preliminary studies indicate that some degree of MPI wavelength selectivity which would allow isomer-specific analysis of PACs is possible. Future work should be directed toward establishing analytical protocols for target molecules, such as the 6-nitro- and 7-nitro-benzocoumarin (nitro-phenanthrene lactone) isomer pair.

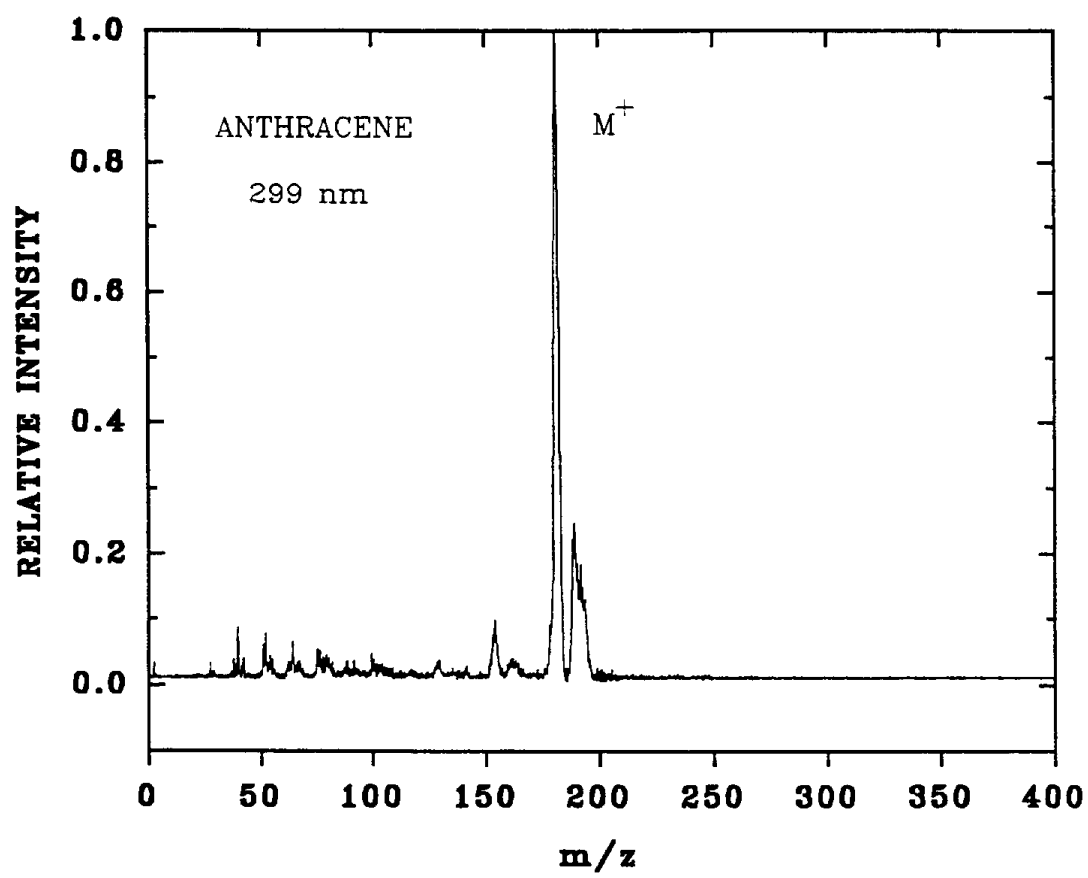
5. REFERENCES

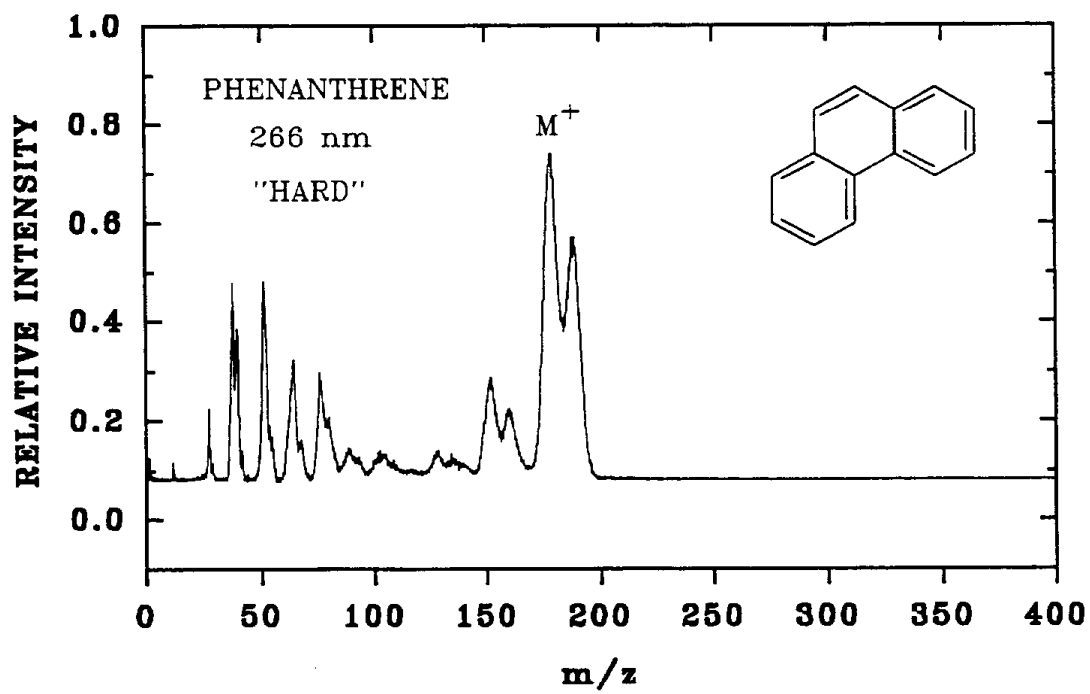
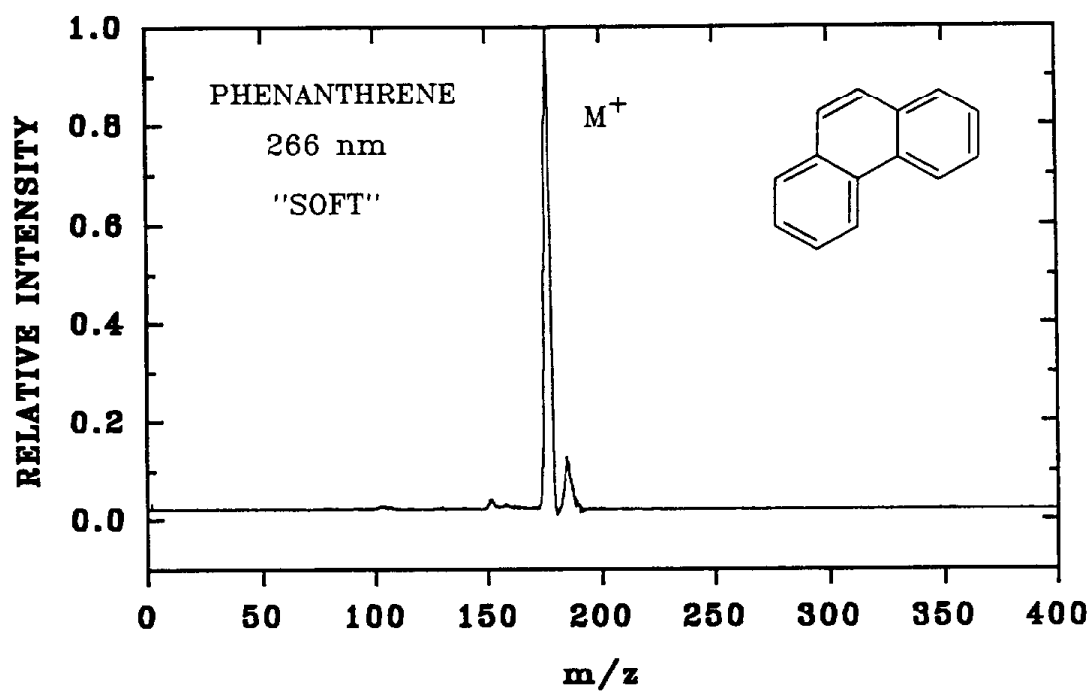
- (1) Zenobi, R., and Zare, R.N., in "Advances in Multi-Photon Processes and Spectroscopy", S.H. Lin, ed. (World Scientific, Singapore, 1991) Vol. 7, pp. 3-167.
- (2) Young, M.K., Jones, A.D., and Kelly, P.B., Proceedings of the 39th ASMS Conference on Mass Spectrometry and Allied Topics, Nashville, TN, May 19-24, 1991. p. 342.
- (3) Zenobi, R., Hahn, J.H., and Zare, R.N., Chem. Phys. Lett. **150**, 361 (1988)
- (4) Lee, M.L., Novotny, M.V., and Bartle, K.D., "Analytical Chemistry of Polycyclic Aromatic Compounds" (Academic Press, New York, 1981) Ch. 8.
- (5) Hagen, D.A., and Eland, J.H.D., Rapid Comm. Mass Spec. **5**, 512-517 (1991)

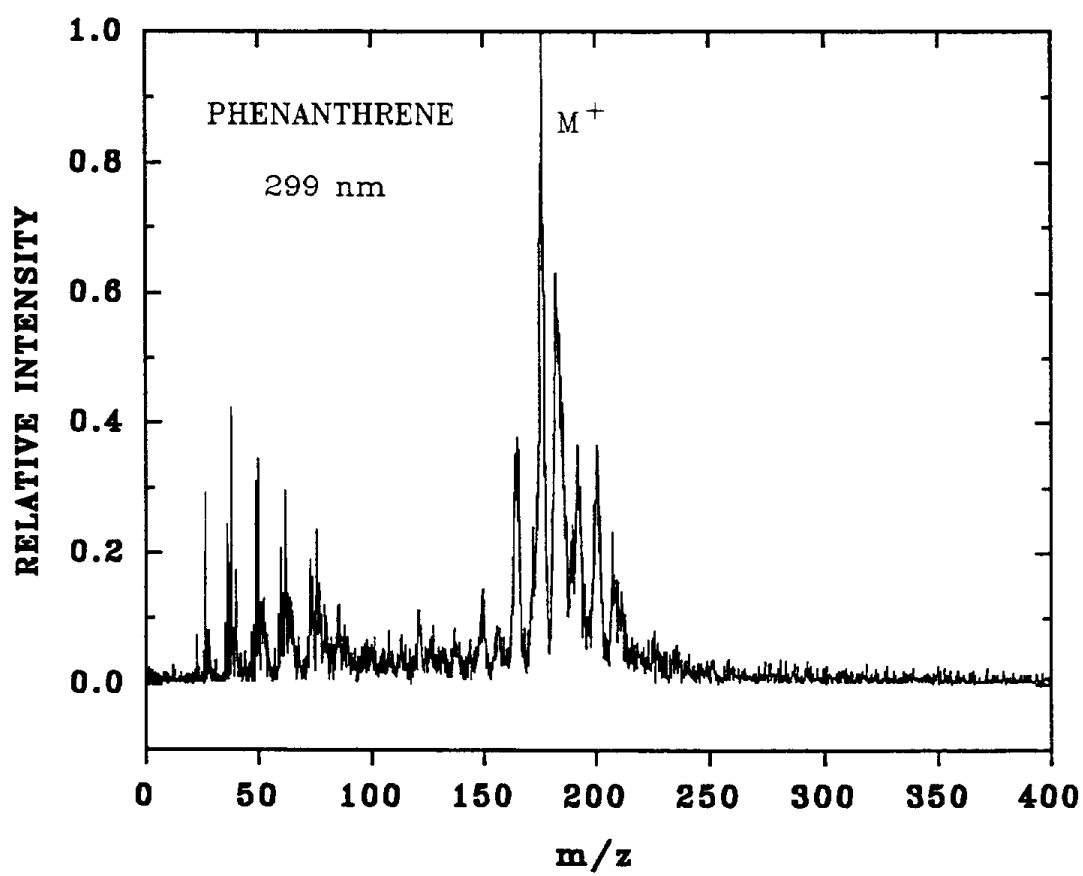
APPENDIX I

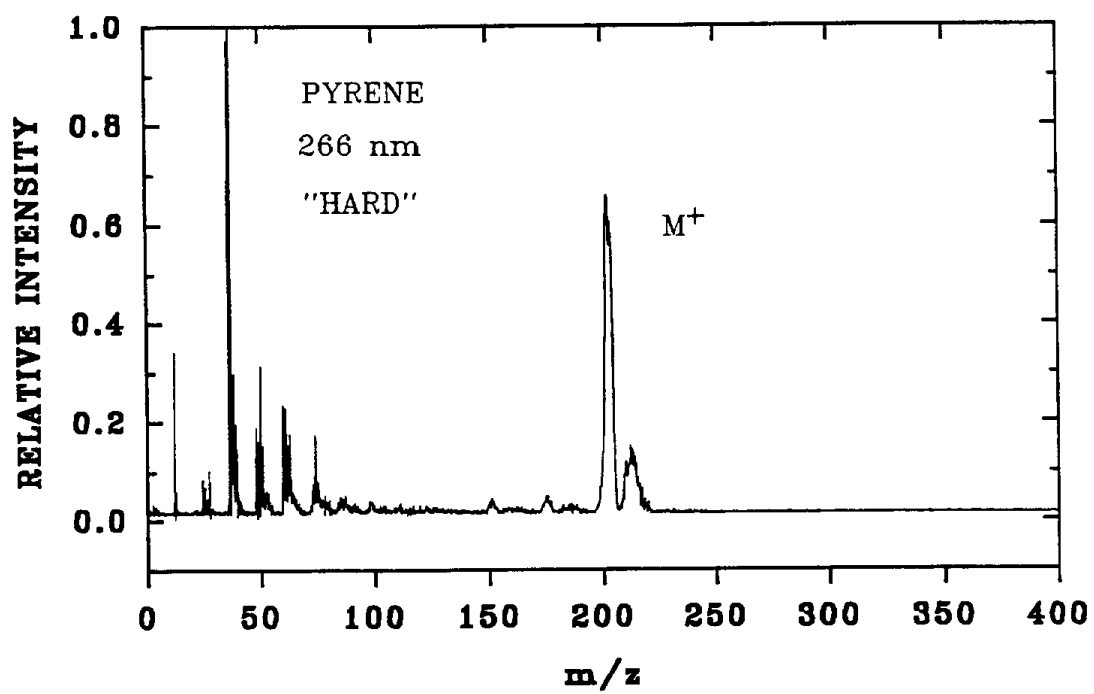
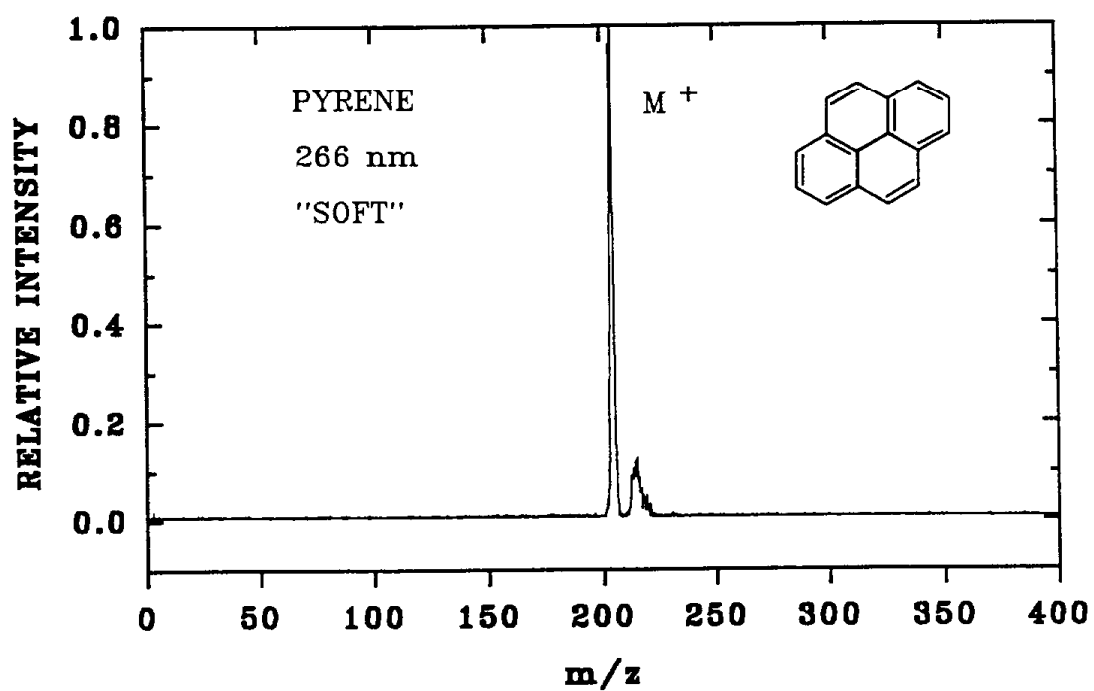
LDLPMS SPECTRA OF STANDARD PAH COMPOUNDS

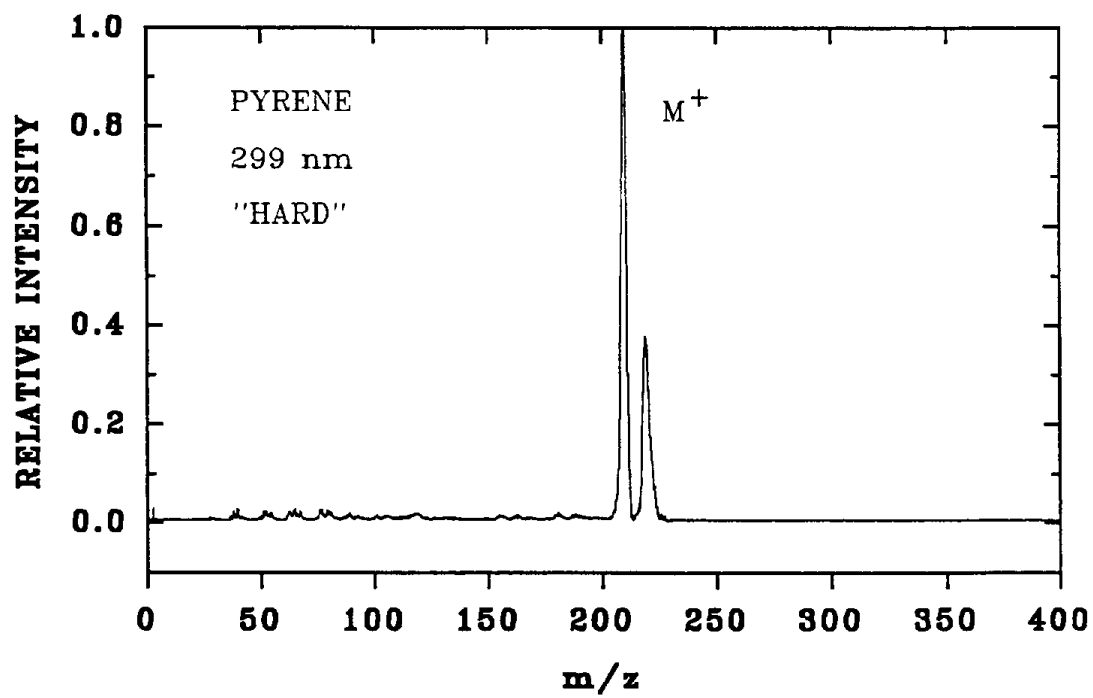
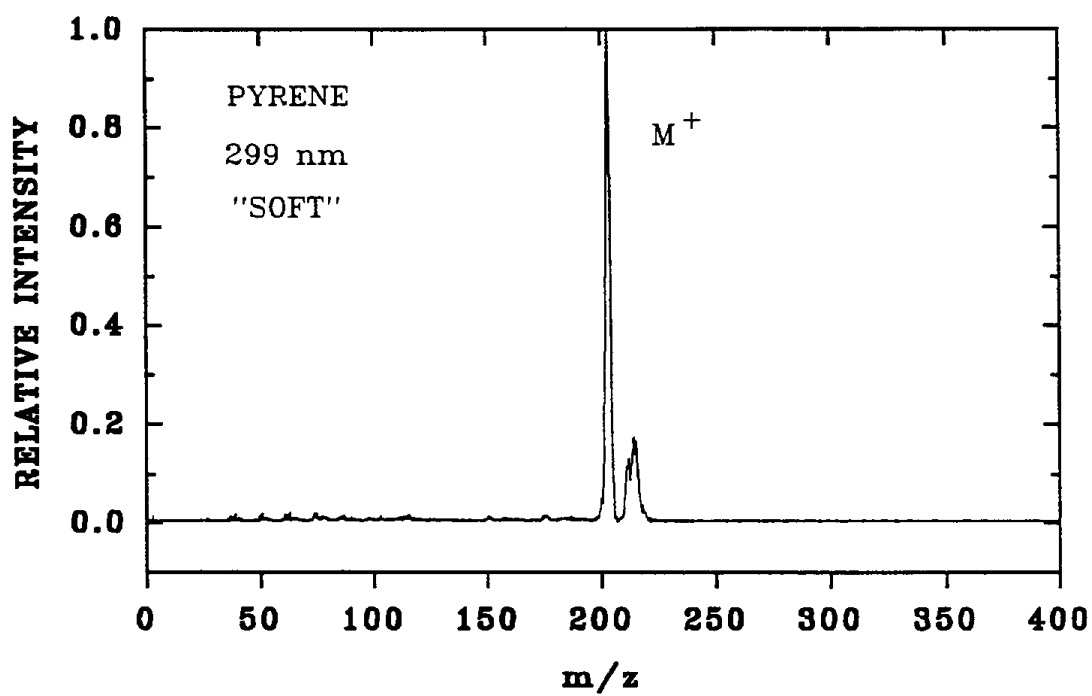


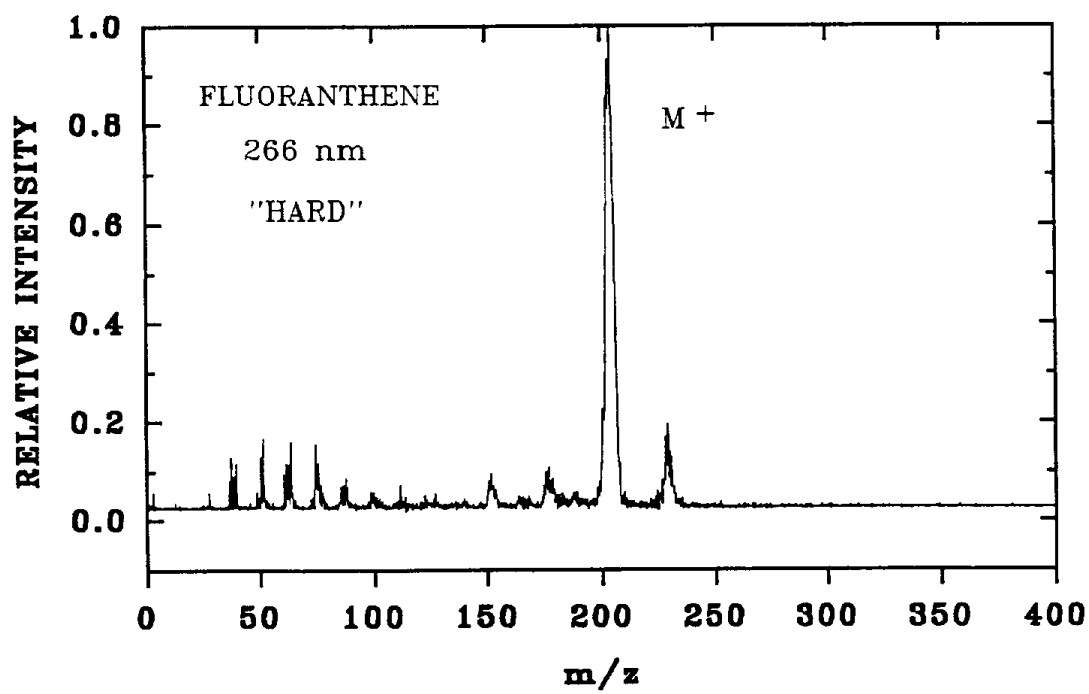
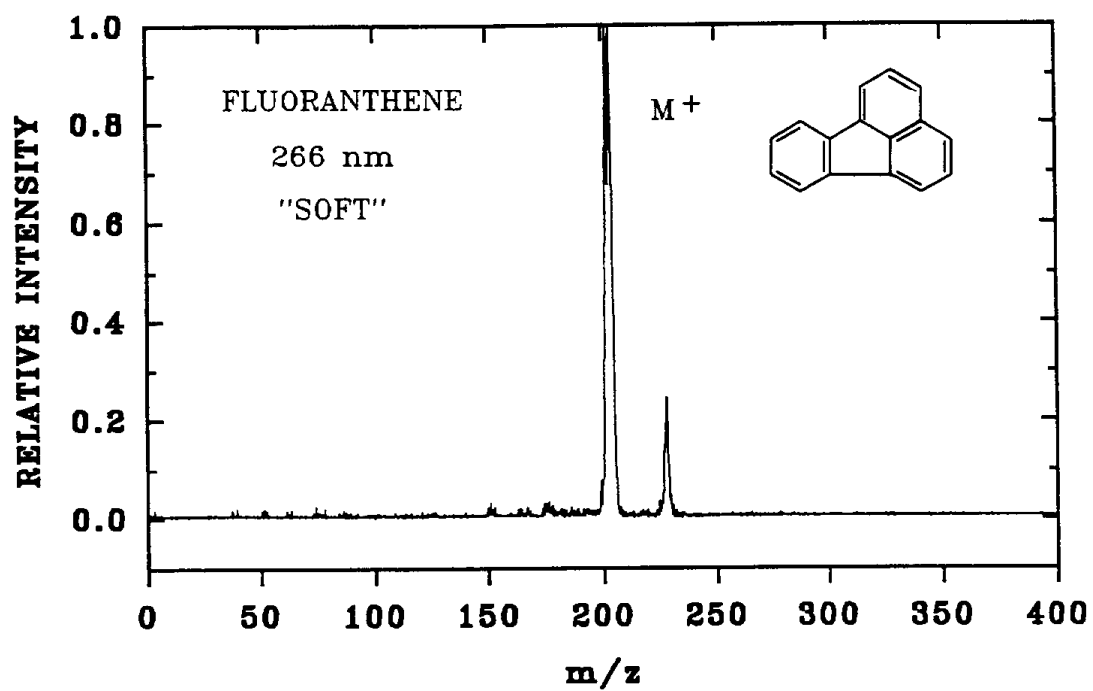


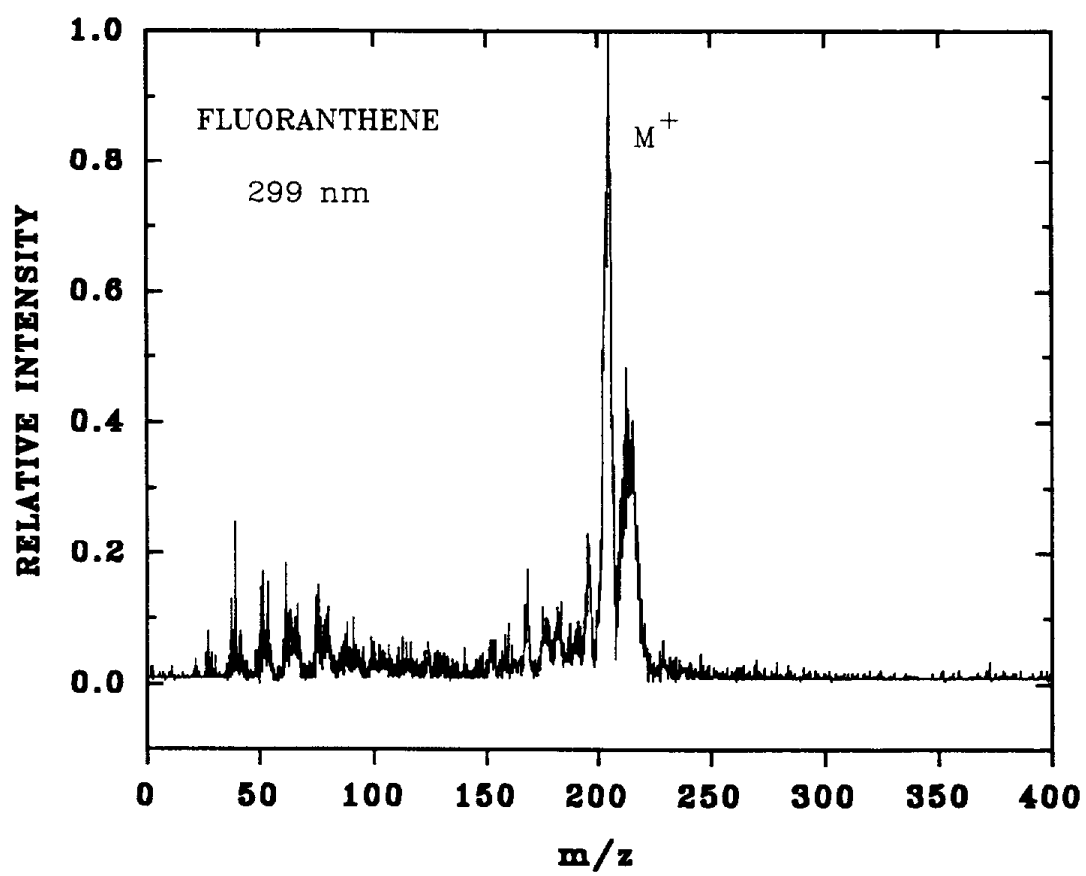


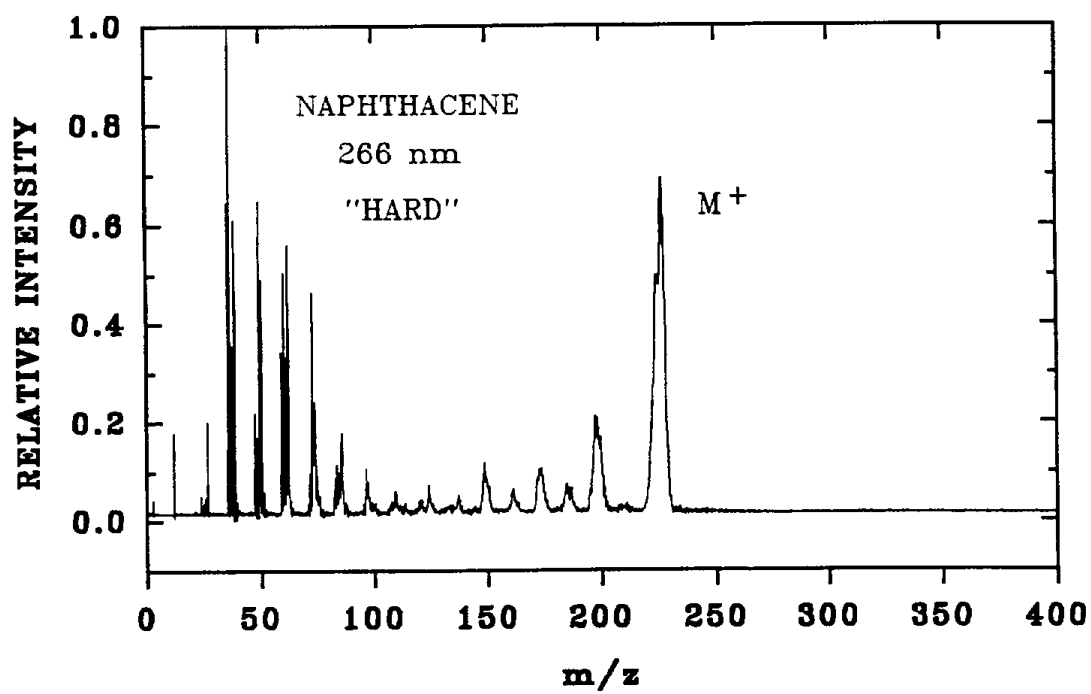
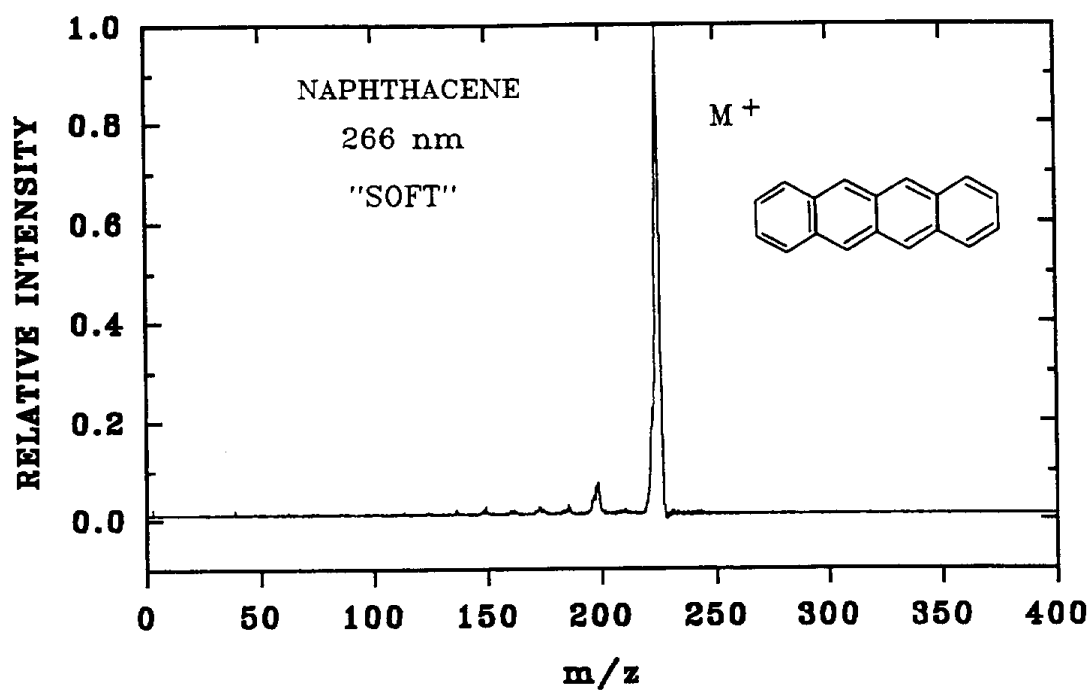


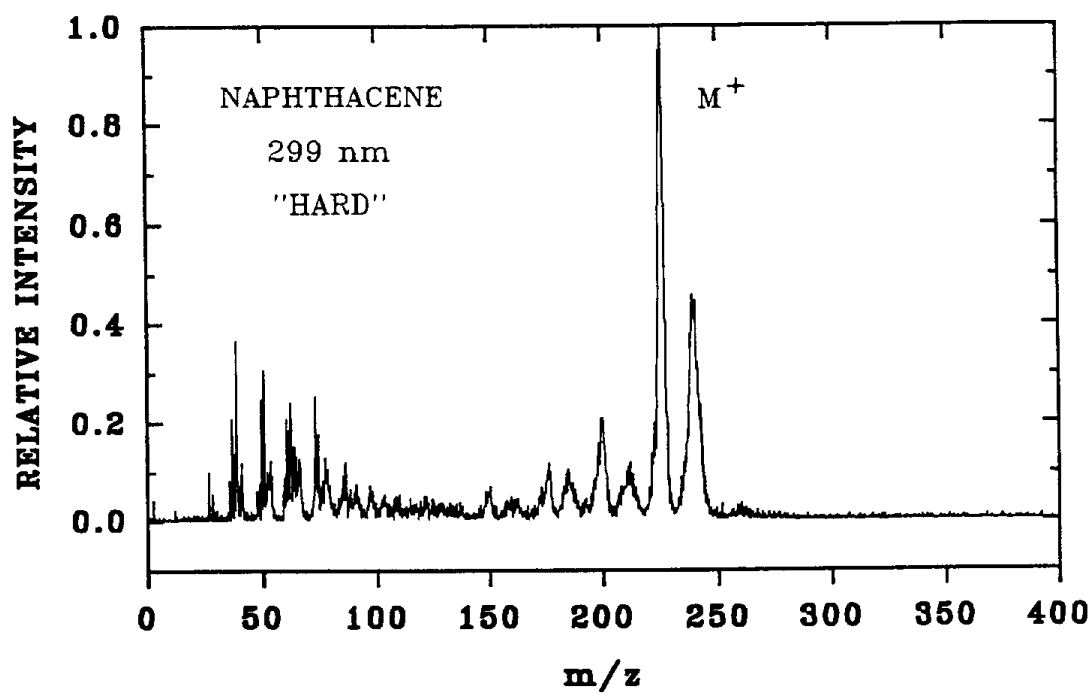
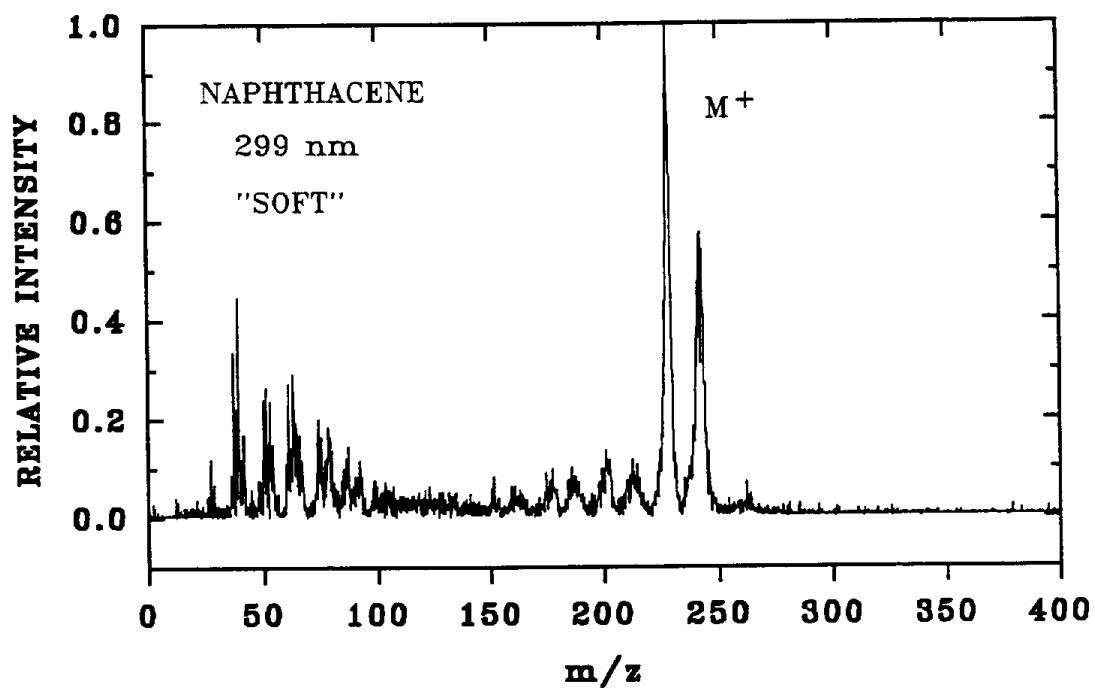


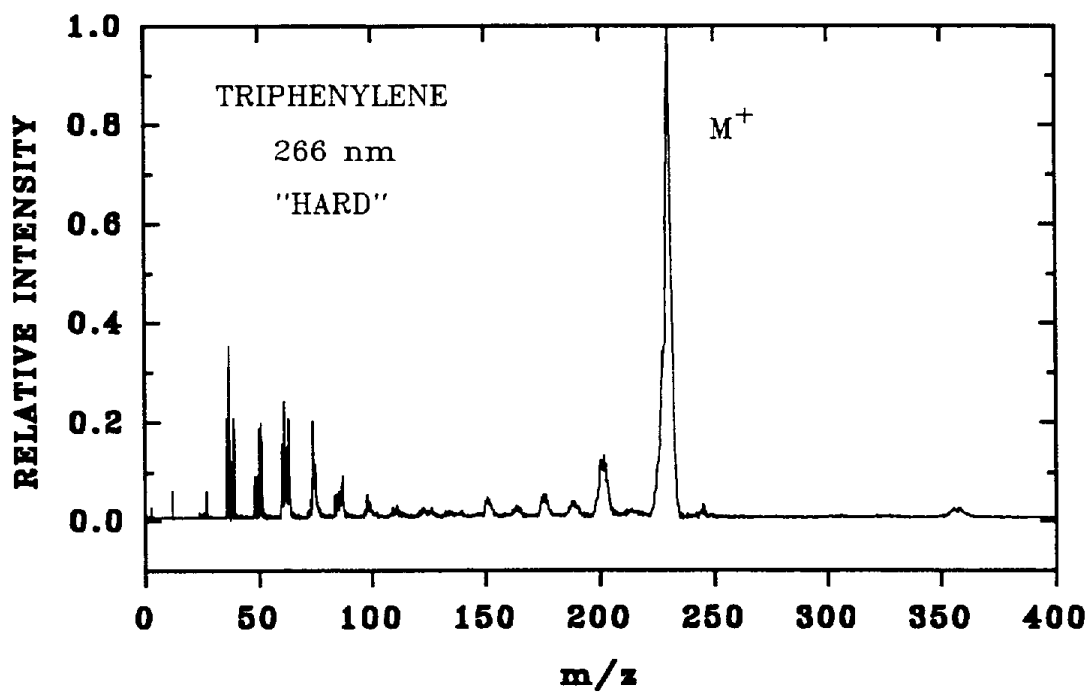
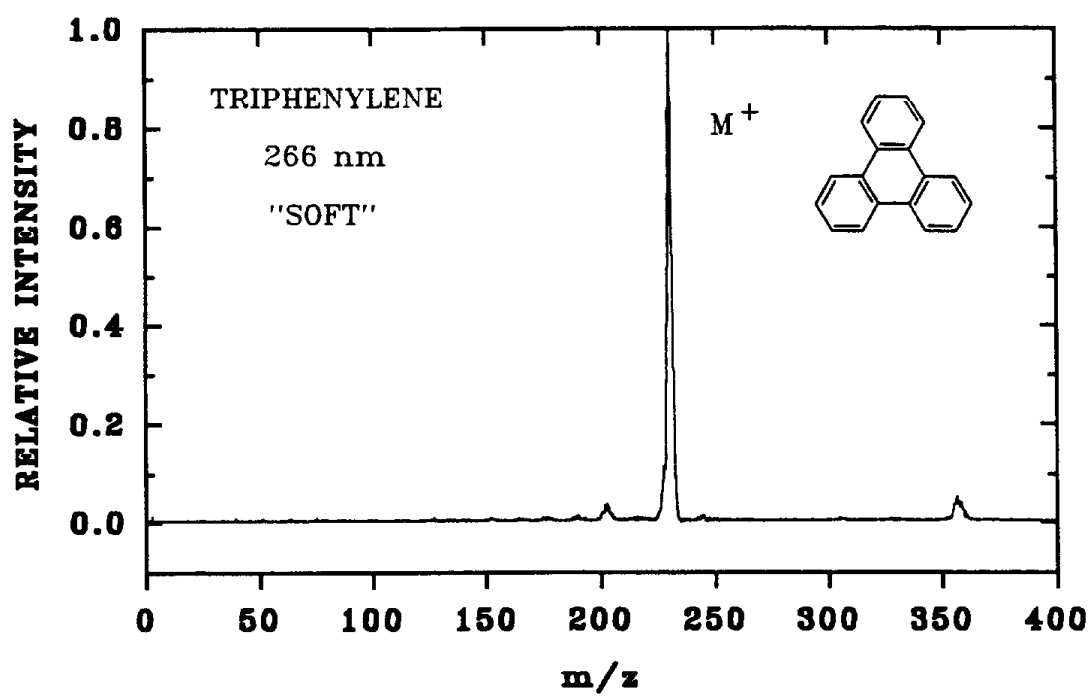


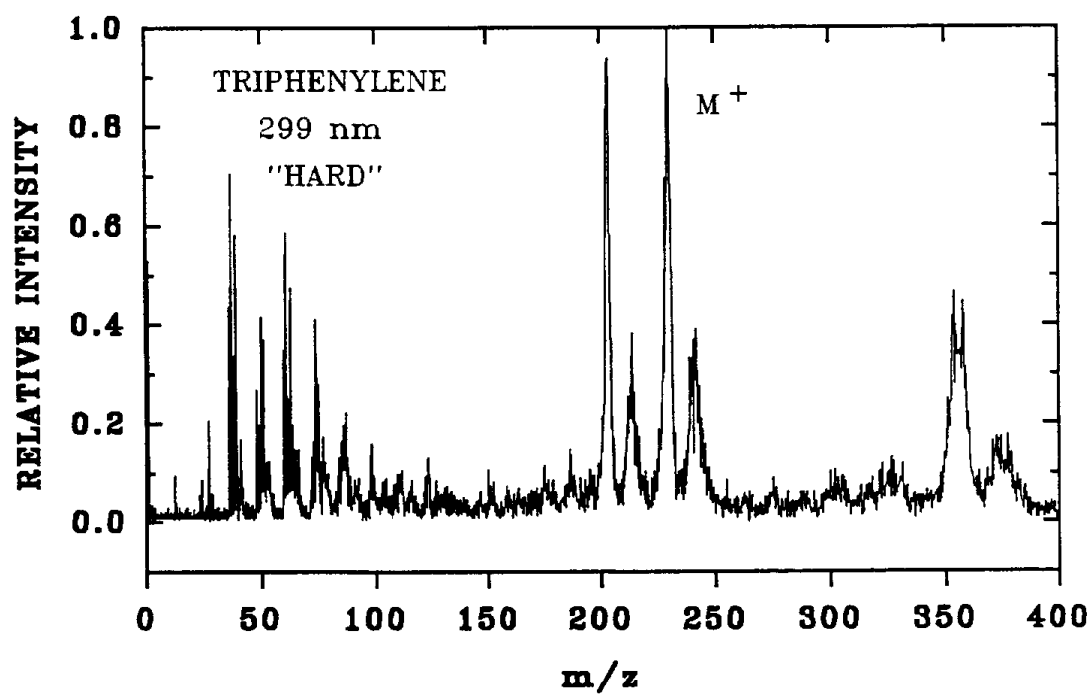
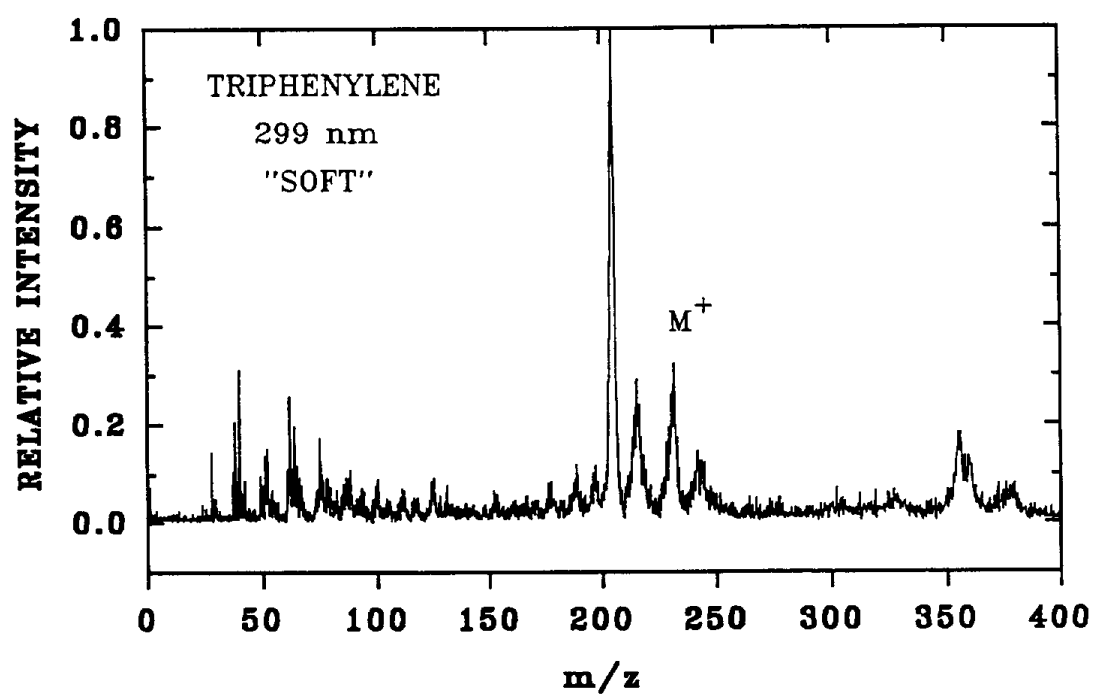


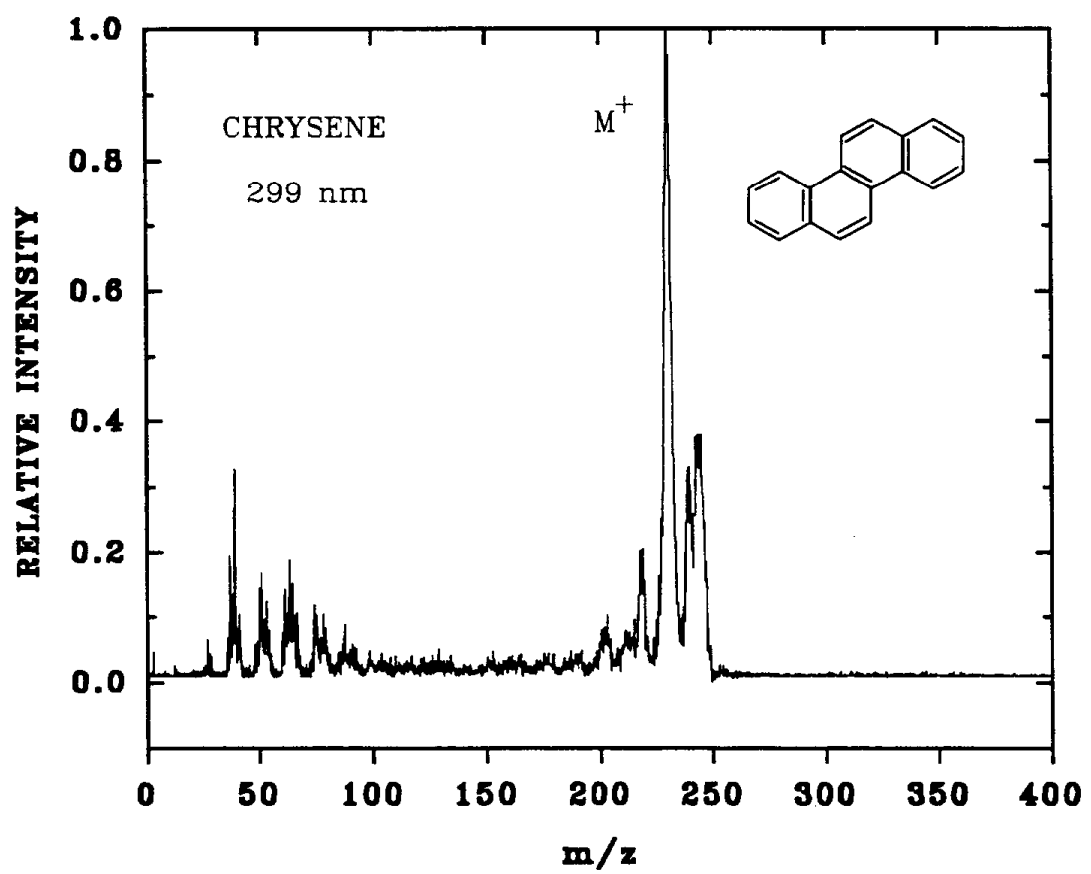


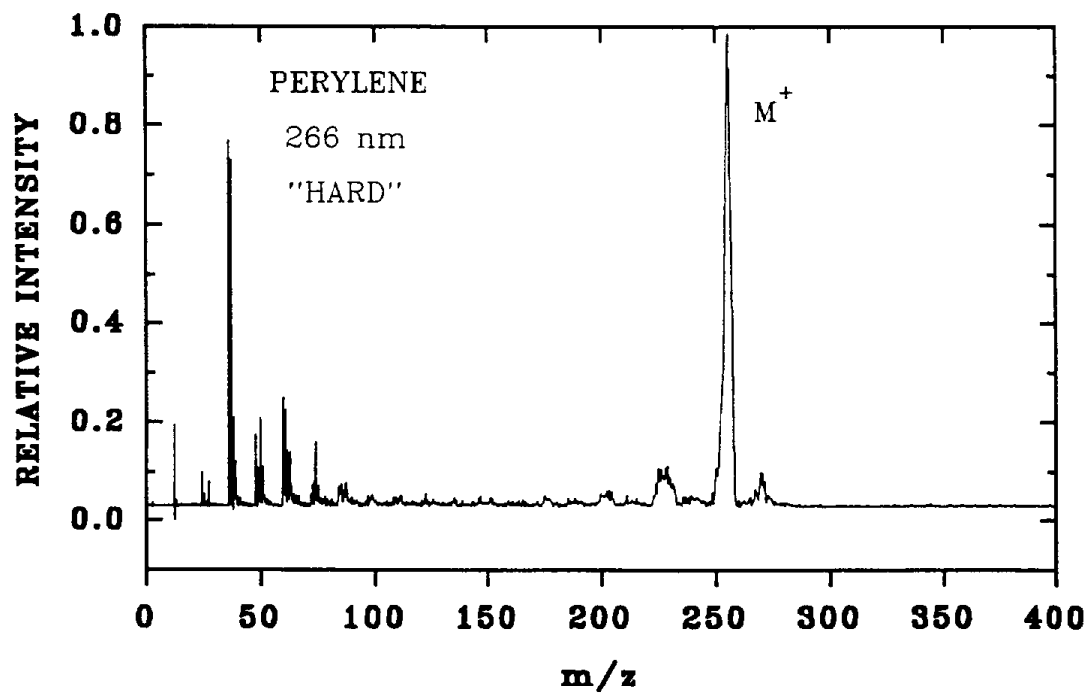
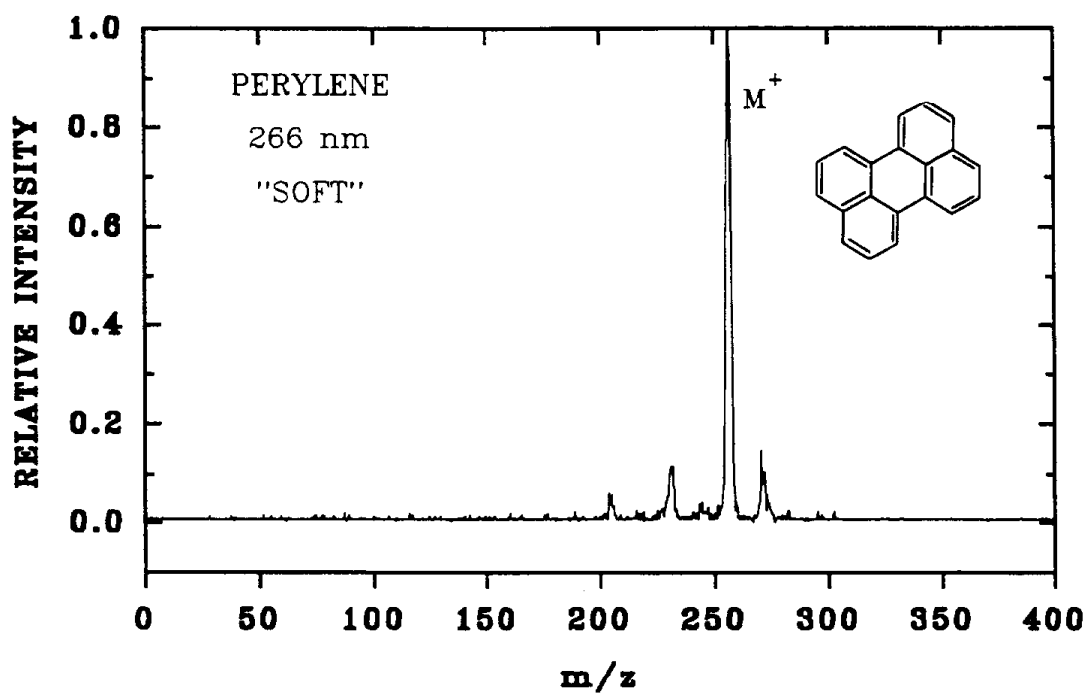


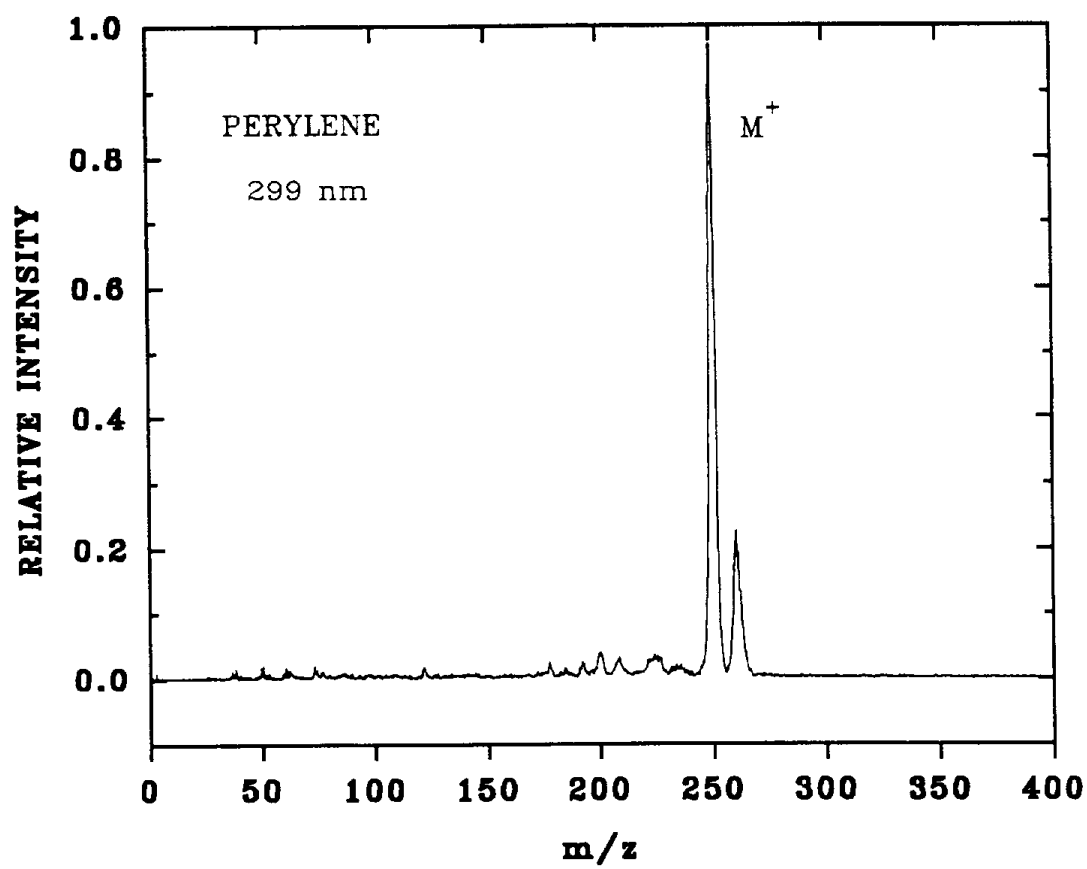


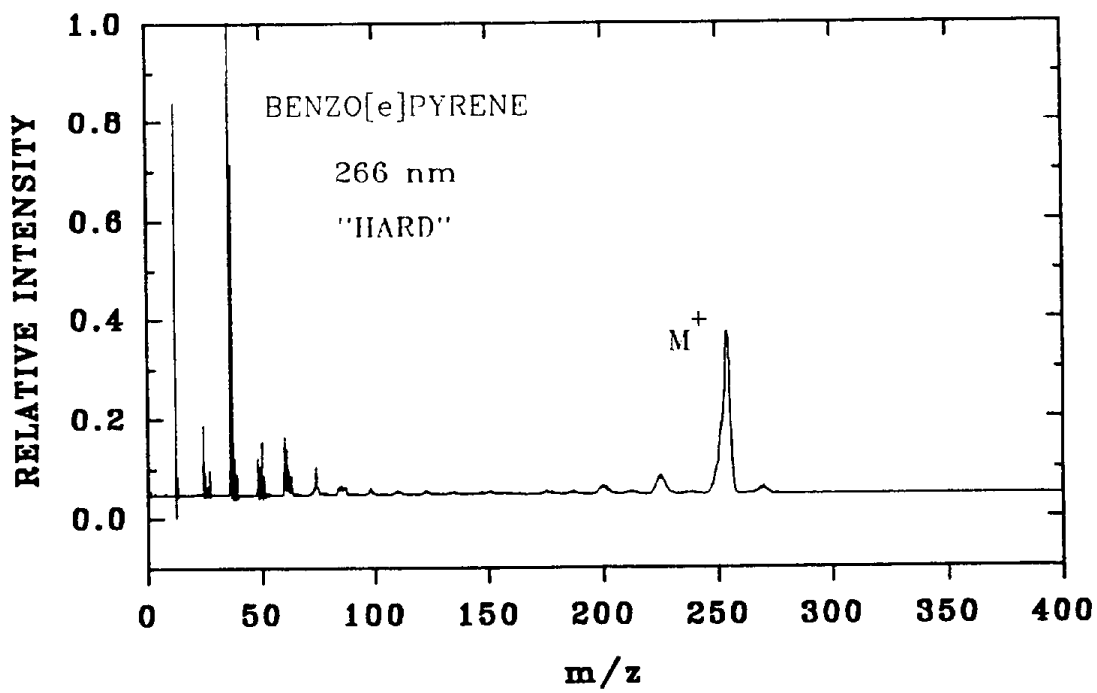
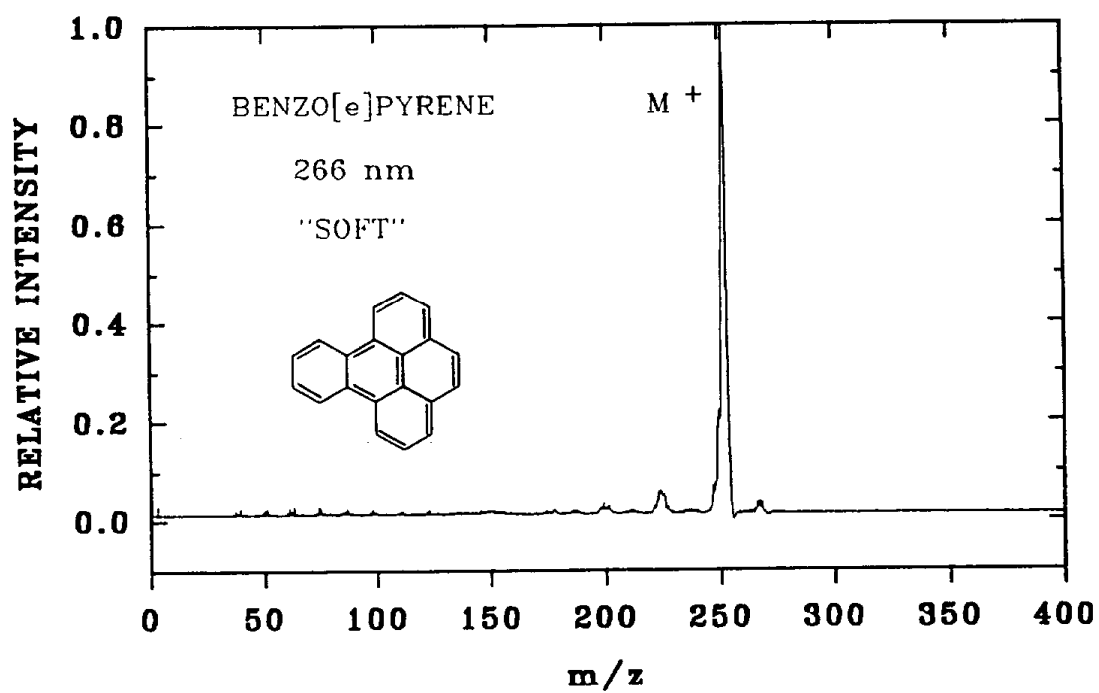


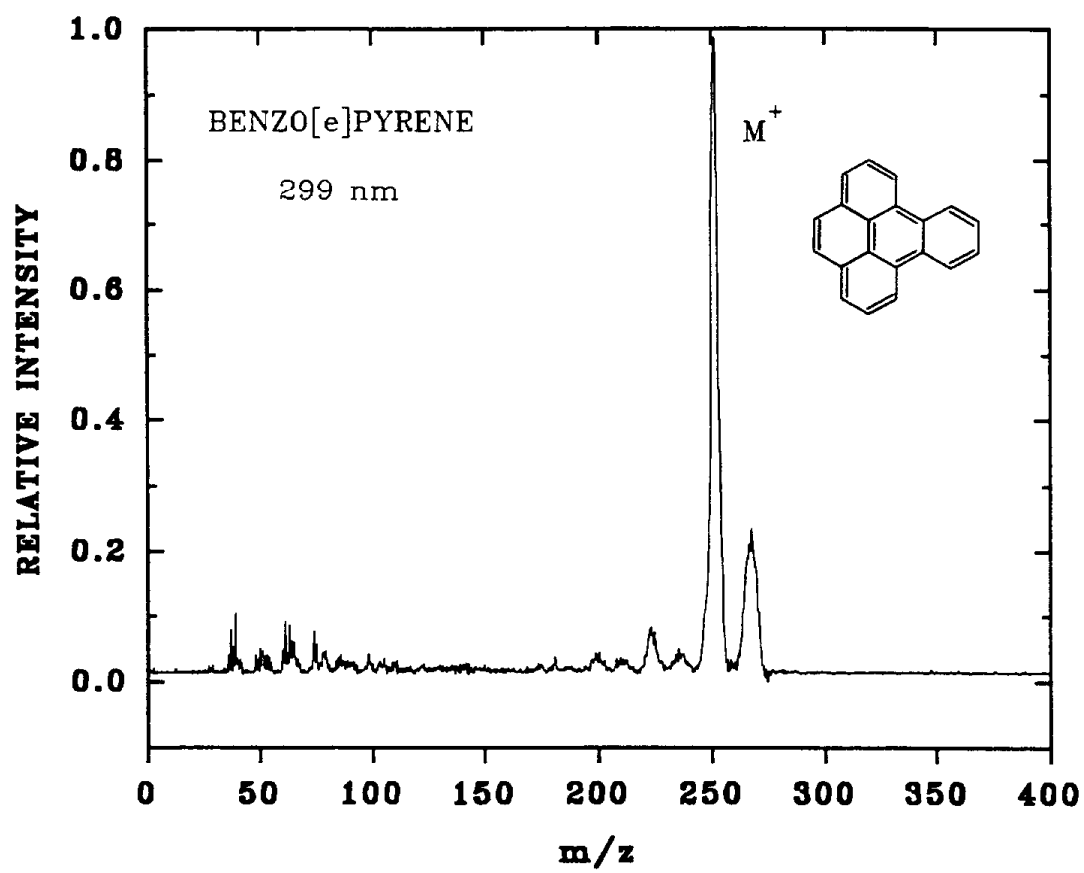


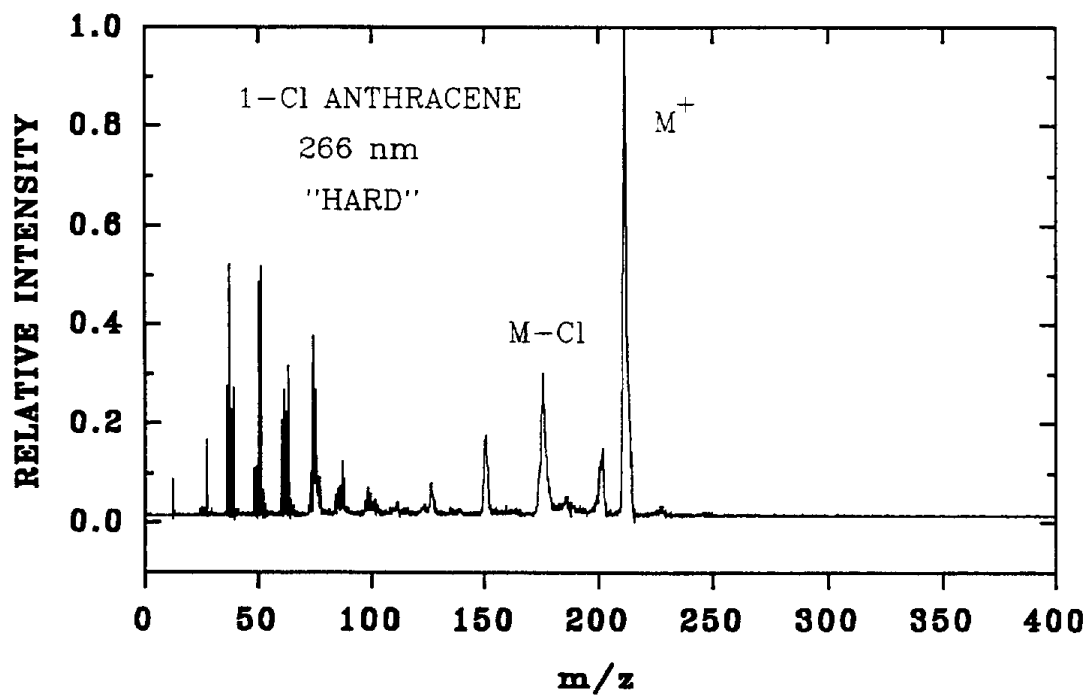
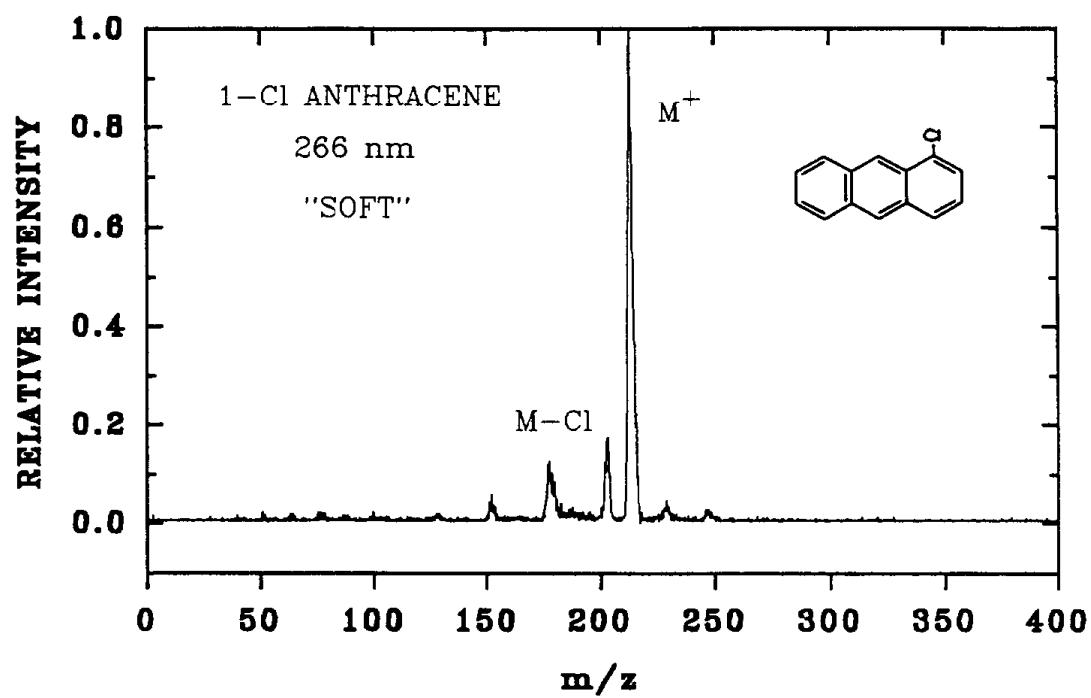


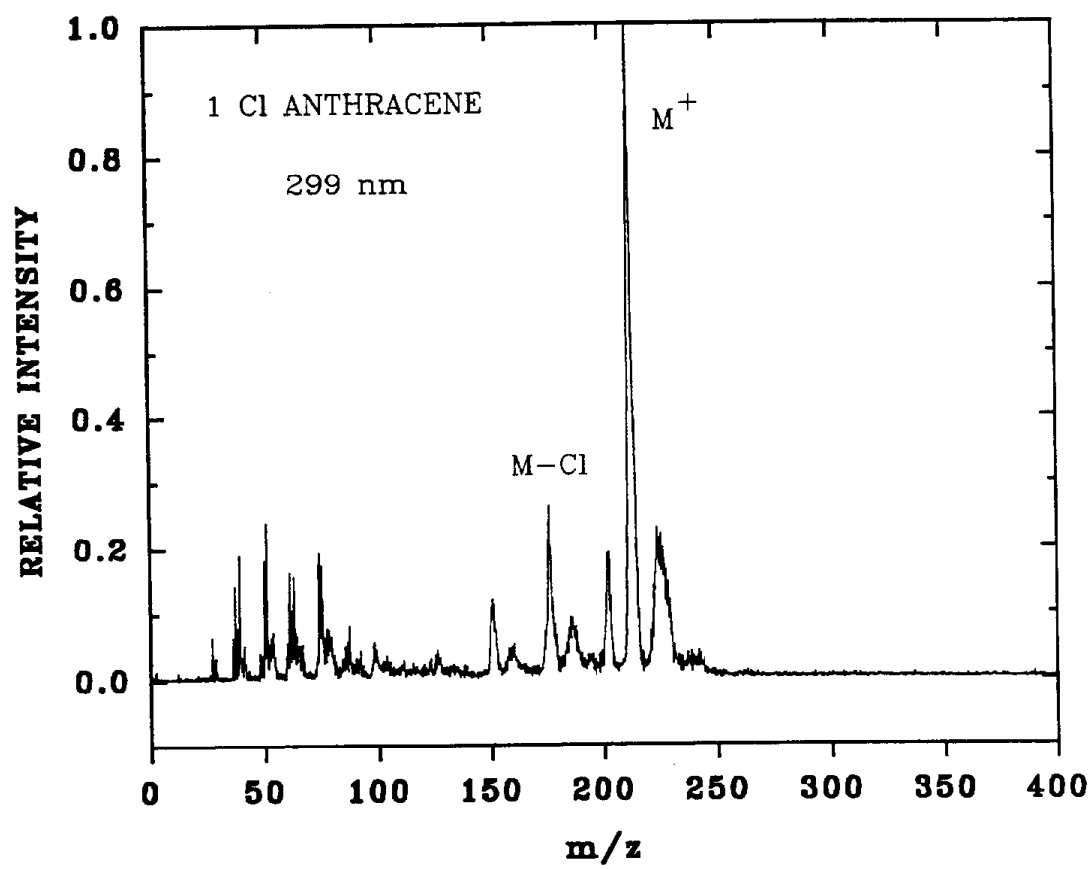


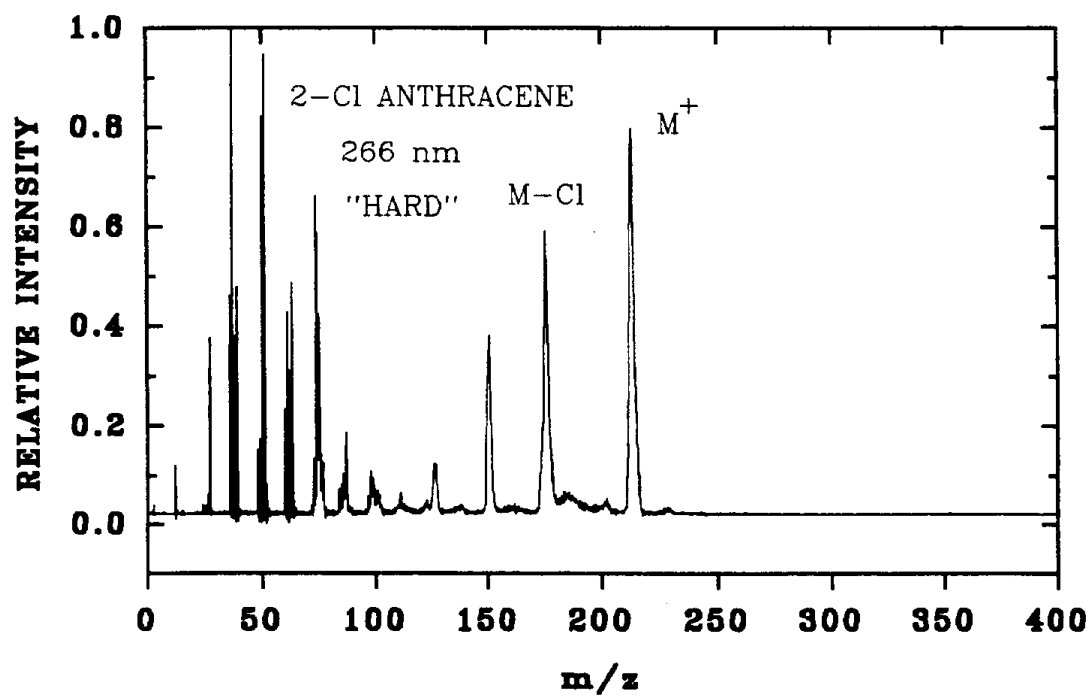
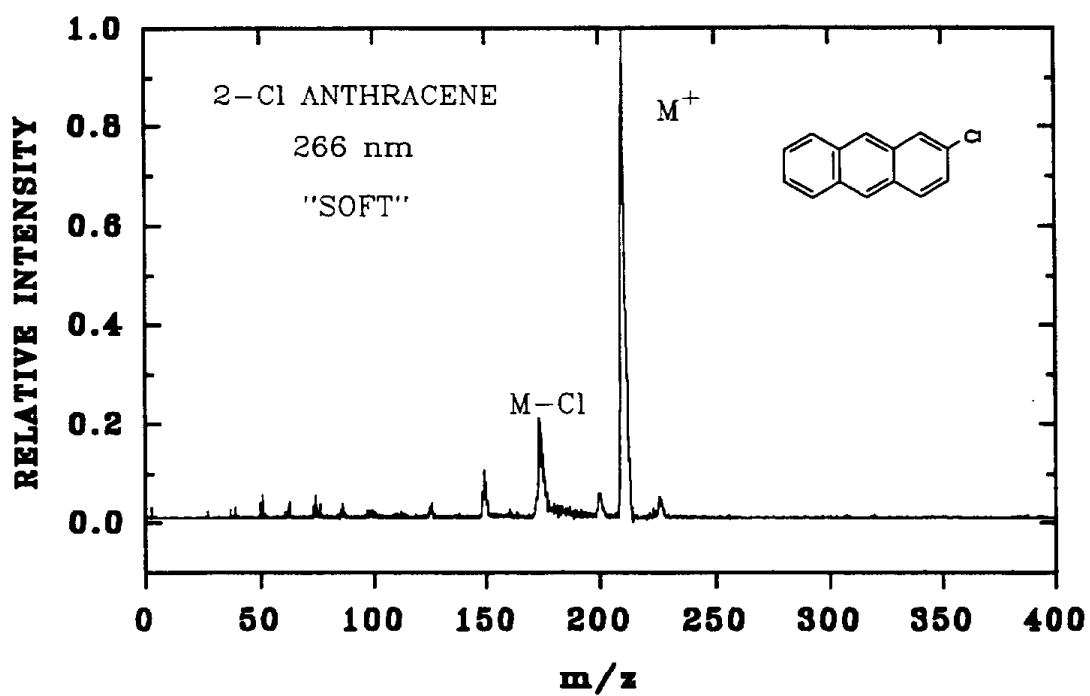












APPENDIX II

GC/MS OF RICE SOOT EXTRACT

A comparison analysis of a rice straw soot extract was performed by conventional GC/MS analysis for PAH at the Facility for Advanced Instrumentation (FAI) by Dr. A.D. Jones. This Appendix contains the total ion chromatogram (TIC) and selected ion integrations (SII) that were used to assist in the identification of PAH in the samples.

A Hewlett Packard 5890 GC equipped with a 15 meter, 0.25 mm i.d. DB-5 fused silica capillary column and interfaced to a VG Trio 2 mass spectrometer was used to perform the analysis. The injector temperature was 275°C and the transfer line temperature was 285°C. The column was held at 40°C for 1 minute prior to ramping at 25°C/min to 200°C. The temperature was then ramped at 4°C/min to a final temperature of 285°C. Helium was used as the carrier gas at a flow rate of 35 cm/sec.

Figure App-II.1 is the TIC of a 0.4 mL extract of the rice straw soot filter sample. The VG Trio data analysis system displays the chromatogram normalized to 100% of the largest peak. Figure App-II.2a is the same TIC reduced in size for comparison with Figures App-II.2b through 2i, which are SII's of specific molecular weight PAH parent molecular ions: 2b, $m/z = 128$; 2c, $m/z = 166$; 2d, $m/z = 178$; 2e, $m/z = 202$; 2f, $m/z = 228$; 2g, $m/z = 252$; 2h, $m/z = 276$; and 2i, $m/z = 278$.

Note that although the molecular weights corresponding to the parent PAH ions 128, 166, 178, and 252 were present in the sample, subsequent analysis of the retention times and ion spectra indicated that these did not correspond to detectable levels of PAH species. The parent ions 276 and 278 were not detected. Two PAH species were identified with ion peaks and corresponded to fluoranthene ($m/z = 202$) and chrysene ($m/z = 228$). Both of these species were near the detection limit of the low resolution analysis performed (about 31 ion counts in each case) and did not appear as distinctive peaks in the TIC. Nevertheless, as discussed in the LDLPMS analysis of rice straw soot samples, $m/z = 202$ was readily detected and also contained lesser quantities of $m/z = 228$ along with other PAH parent ions (see Figures 17 and 19 in the main body of the report and LDLPMS spectra for fluoranthene and chrysene in Appendix I). Thus we conclude that the LDLPMS analyses have sensitivities comparable to or greater than conventional low resolution GC/MS.

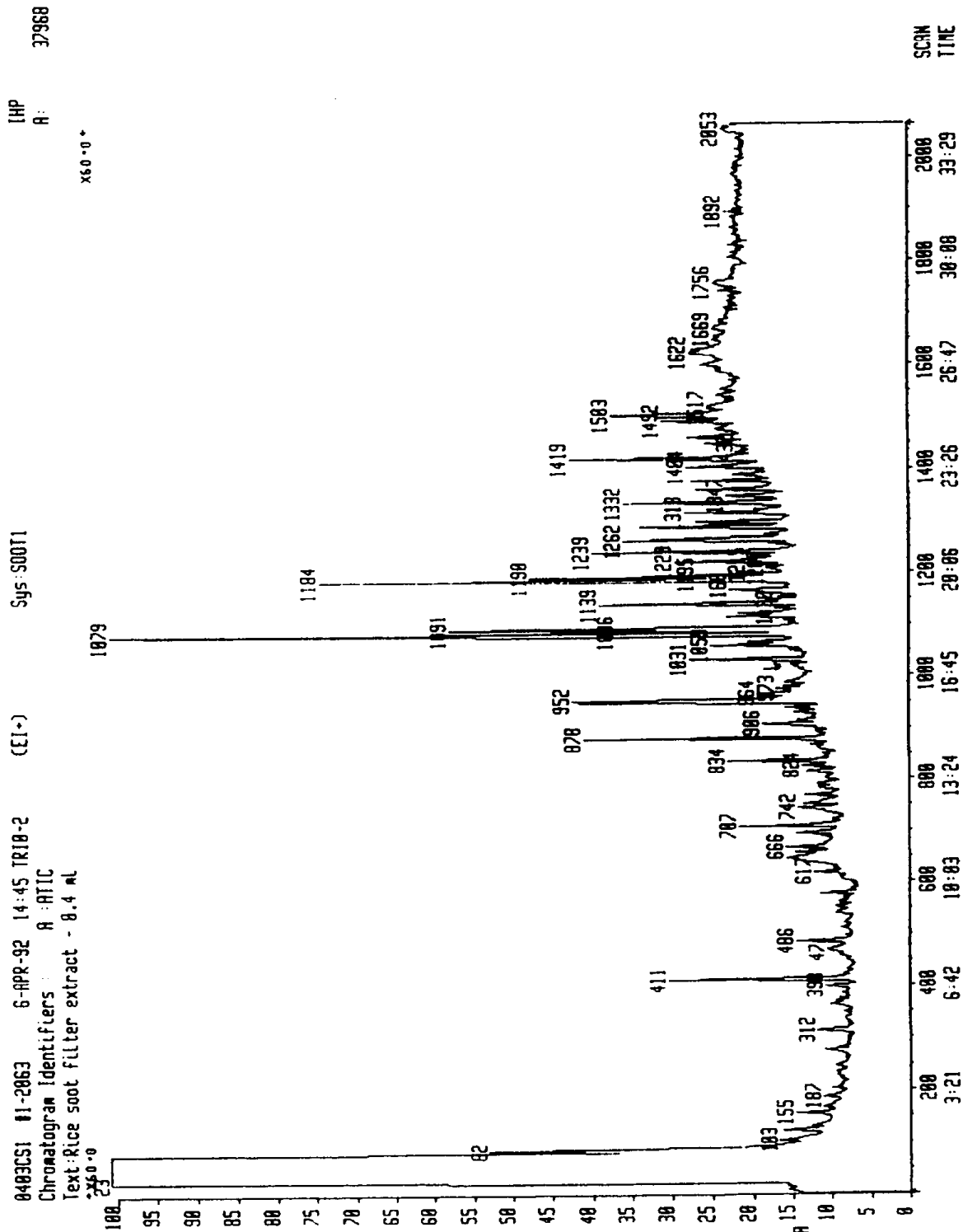
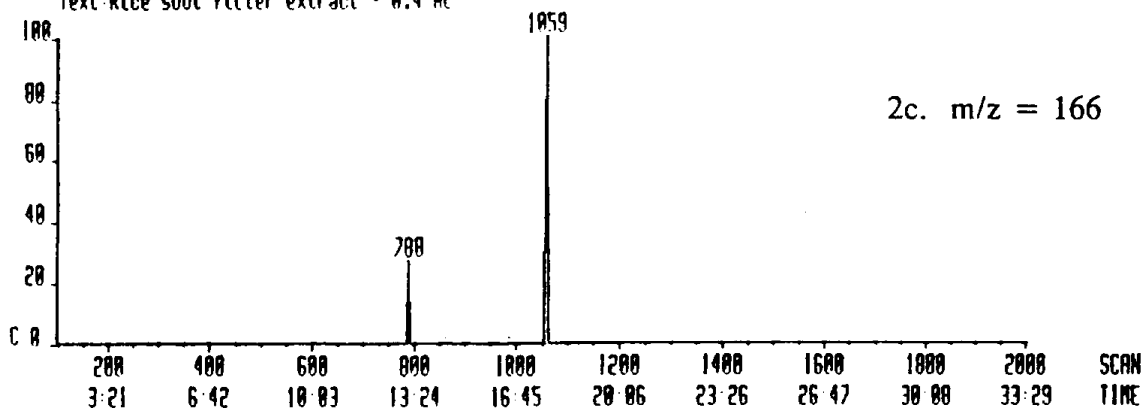
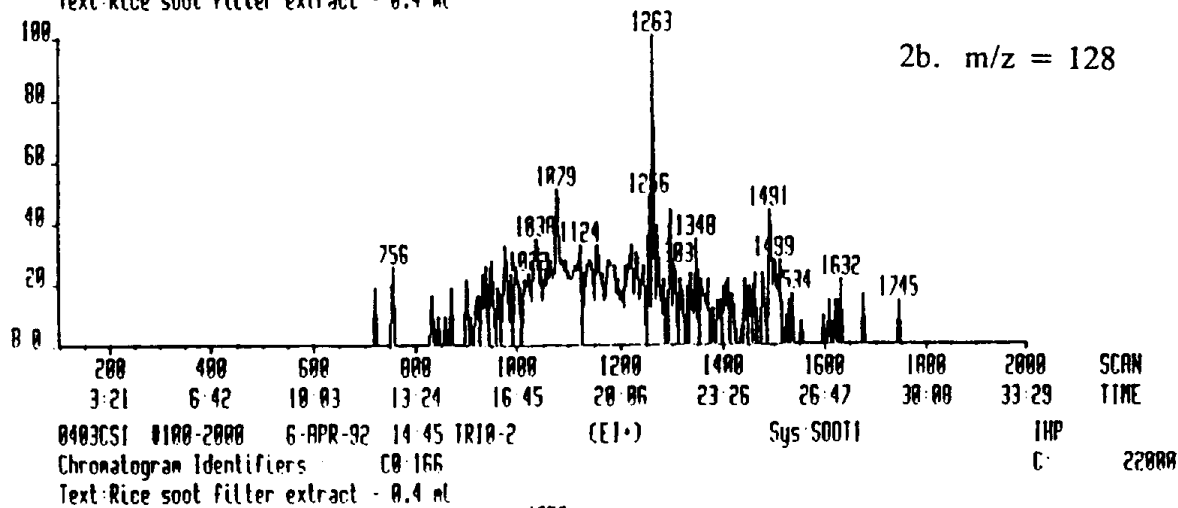
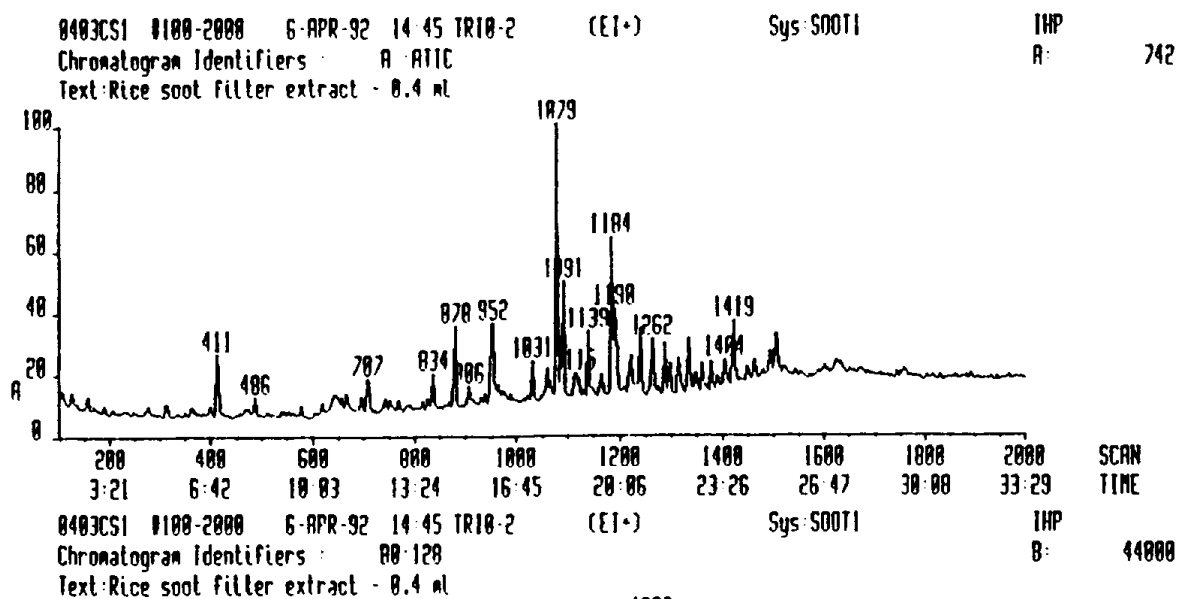


FIGURE APP-II.1 TIC of rice straw soot filter extract.

FIGURE APP-II.2a TIC of rice straw soot filter extract.



0403CSI 0100-2000 6-APR-92 14 45 TR10-2

(EI+)

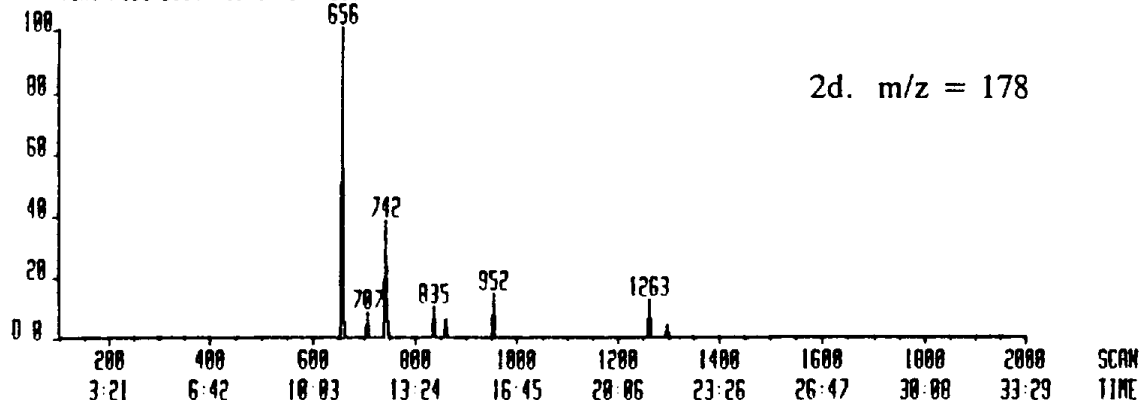
Sys: S00T1

1HP

Chromatogram Identifiers : 00:170

0: 90000

Text: Rice soot filter extract - 0.4 ml



0403CSI 0100-2000 6-APR-92 14 45 TR10-2

(EI+)

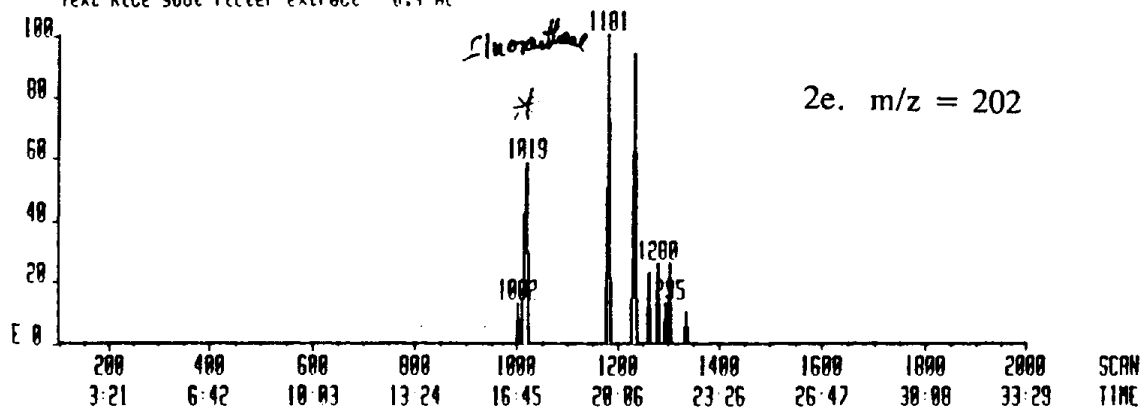
Sys: S00T1

1HP

Chromatogram Identifiers : 00:202

E: 31000

Text: Rice soot filter extract - 0.4 ml



0403CSI 0100-2000 6-APR-92 14 45 TR10-2

(EI+)

Sys: S00T1

1HP

Chromatogram Identifiers : 00:220

E: 31000

Text: Rice soot filter extract - 0.4 ml

